AD-A124 991 SCINTILLATION ANALYSIS OF GAMMA RADIATION WITH CRYSTALS 1/1
OF BISMUTH GERMANATE(U) NAVAL POSTGRADUATE SCHOOL
MONTEREY CA R R COOKE OCT 82

UNCLASSIFIED . F/G 20/2 NL

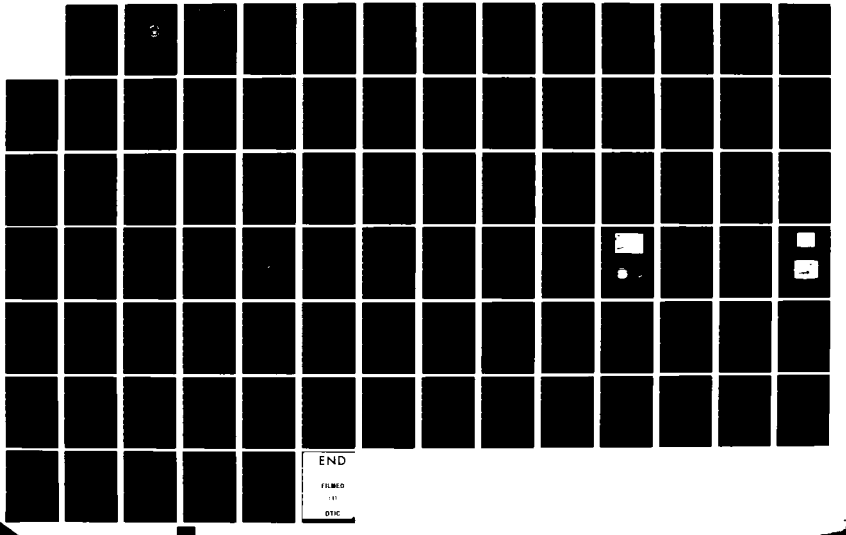

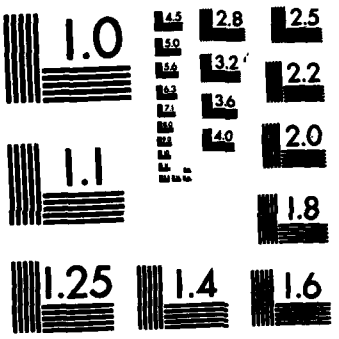

MICROCOPY RESOLUTION TEST CHART
NATIONAL BUREAU OF STANDARDS-1963-A

NAVAL POSTGRADUATE SCHOOL
Monterey, California

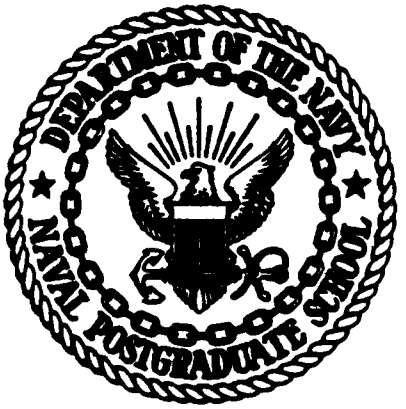

THESIS

SCINTILLATION ANALYSIS OF GAMMA RADIATION WITH CRYSTALS OF BISMUTH GERMANATE

by

Robert R. Cooke

October 1982

Thesis Advisor: F. R. Buskirk

Approved for public release; distribution unlimited.

UNCLASSIFIED

SECURITY CLASSIFICATION OF THIS PAGE (When Data Entered)

REPORT DOCUMENTATION PAGE	READ INSTRUCTIONS BEFORE COMPLETING FORM
1. REPORT NUMBER	2. GOVT ACCESSION NO. AD-A124 994 / 3. RECIPIENT'S CATALOG NUMBER
4. TITLE (and Subtitle) Scintillation Analysis of Gamma Radiation with Crystals of Bismuth Germanate	5. TYPE OF REPORT & PERIOD COVERED Master's Thesis; October 1982
	6. PERFORMING ORG. REPORT NUMBER
7. AUTHOR(s) Robert R. Cooke	8. CONTRACT OR GRANT NUMBER(s)
9. PERFORMING ORGANIZATION NAME AND ADDRESS Naval Postgraduate School Monterey, California 93940	10. PROGRAM ELEMENT, PROJECT, TASK AREA & WORK UNIT NUMBERS
11. CONTROLLING OFFICE NAME AND ADDRESS Naval Postgraduate School Monterey, California 93940	12. REPORT DATE October 1982
	13. NUMBER OF PAGES 86
14. MONITORING AGENCY NAME & ADDRESS(if different from Controlling Office)	15. SECURITY CLASS. (of this report) Unclassified
	15a. DECLASSIFICATION/DOWNGRADING SCHEDULE

16. DISTRIBUTION STATEMENT (of this Report)

Approved for public release; distribution unlimited.

17. DISTRIBUTION STATEMENT (of the abstract entered in Block 20, if different from Report)

18. SUPPLEMENTARY NOTES

19. KEY WORDS (Continue on reverse side if necessary and identify by block number)

Bismuth Germanate

Scintillation

Radiation Damage

20. ABSTRACT (Continue on reverse side if necessary and identify by block number)

This report provides an introduction to the theory of scintillation counting and analysis of nuclear radiation, with particular attention to an application for bismuth germanate ($Bi_4Ge_3O_{12}$), or BGO, scintillator crystals.

Radiation damage experiments using 100 MeV electrons from a linear accelerator were conducted to evaluate the induced

DD FORM 1 JAN 73 1473 EDITION OF 1 NOV 65 IS OBSOLETE S/N 0102-014-6601

UNCLASSIFIED

SECURITY CLASSIFICATION OF THIS PAGE (When Data Entered)

#20 - ABSTRACT - (CONTINUED)

radiation and subsequent resolution capability of bismuth germanate and thallium activated sodium iodide scintillators. It was shown that BGO has a much higher resistance to radiation damage from electron and photon activation sources.

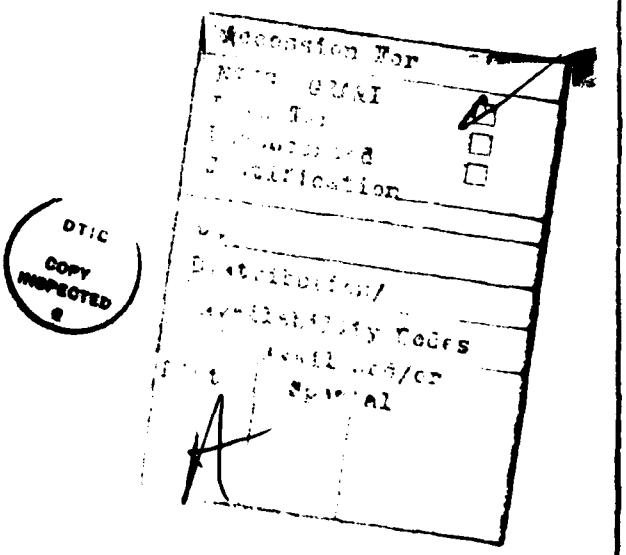

Approved for public release; distribution unlimited.

Scintillation Analysis of Gamma Radiation with Crystals of Bismuth Germanate

by

Robert R. Cooke
Captain, United States Army
B.S., Northeastern University, 1972

Submitted in partial fulfillment of the requirements for the degree of

MASTER OF SCIENCE IN PHYSICS

from the

NAVAL POSTGRADUATE SCHOOL
October 1982

Author: Robert R Cooke

Approved by: Fred R Buskirk
Thesis Advisor

I. Dyer
Second Reader

I. Dyer
Chairman, Department of Physics

William M. Tolles
Dean of Science and Engineering

ABSTRACT

This report provides an introduction to the theory of scintillation counting and analysis of nuclear radiation, with particular attention to an application for bismuth germanate ($Bi_4Ge_3O_{12}$), or BGO, scintillator crystals.

Radiation damage experiments using 100 MeV electrons from a linear accelerator were conducted to evaluate the induced radiation and subsequent resolution capability of bismuth germanate and thallium activated sodium iodide scintillators. It was shown that BGO has a much higher resistance to radiation damage from electron and photon activation sources.

TABLE OF CONTENTS

LIST OF TABLES

LIST OF FIGURES

I. INTRODUCTION

The basic idea of a scintillation counter is to absorb an incident radiation, either electromagnetic or particle, reduce it to a large number of monochromatic photons and then count the number of these photons (scintillations). By multiplying the characteristic photon energy by the total number of photons, one obtains the energy of the incident radiation. This energy value is considered as one counting event. The collection of many (typically millions) counting events yields a number density distribution of energy levels such as in Figure 1. From the determination of energy peaks (e.g., .511 MeV and 1.27 MeV), one can surmise the identity of the source material (e.g., sodium-22) which is irradiating the scintillator. Two basic assumptions are required for this process, and are in fact valid. The first is that only one primary event (cascade shower) at a time is sensed by the detector. The second assumption is that a cascade shower is completed in a short time, and is integrated into a single event by the detection circuits.

Further, it is important that all secondaries resulting from the primary events be captured in the crystal if the photomultiplier signal is to be proportional to the primary energy. In Section III the processes leading from a primary event to an observable signal are studied in more detail.

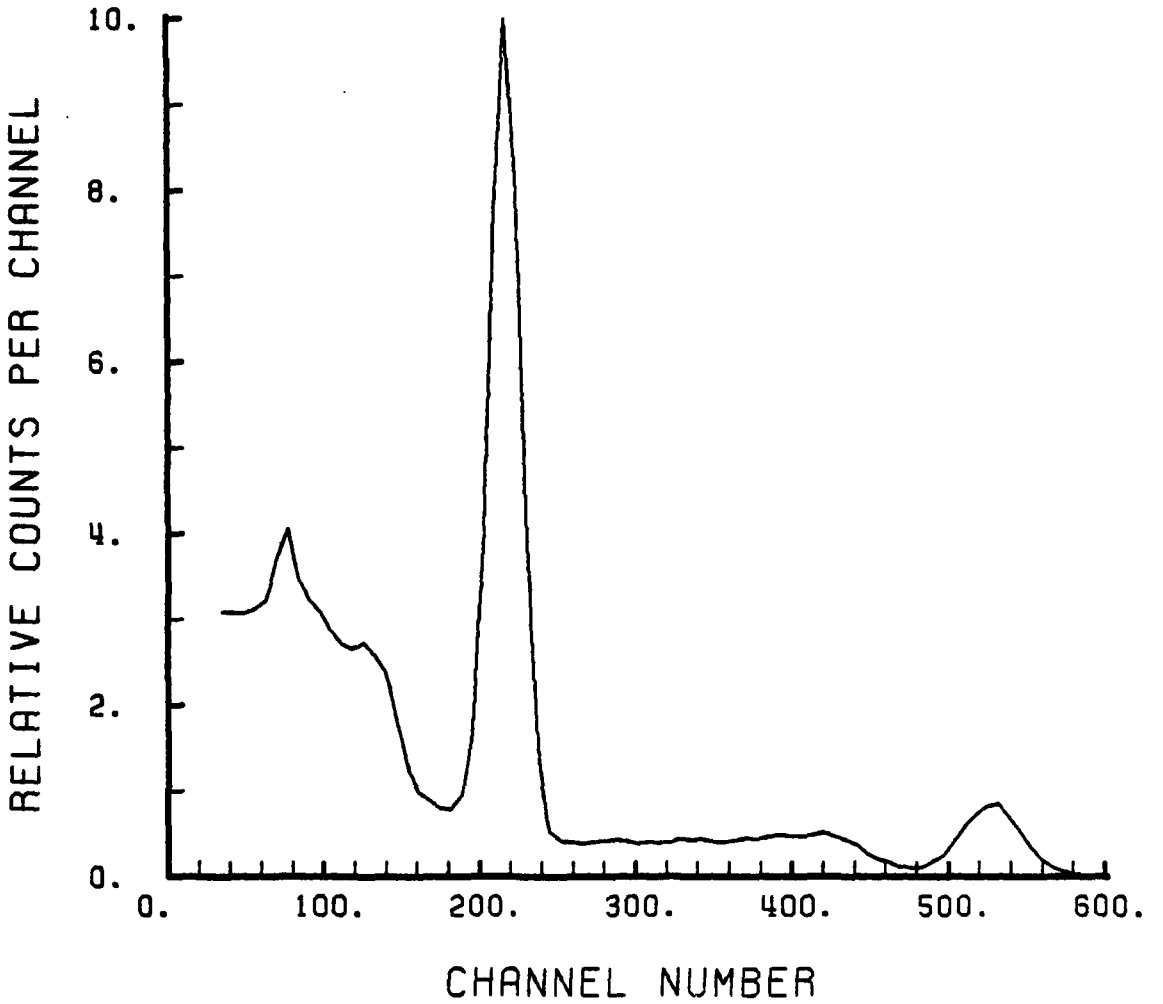

Figure 1. Pulse Height Spectrum of Sodium-22 Using a NaI(Tl) Scintillator

II. HISTORY

The detection of nuclear radiation with scintillation techniques has played an important role in many of the basic experiments of nuclear physics. About 1900, it was observed that alpha particles cause luminescence when they strike certain ("phosphor") materials such as zinc sulfide, barium platino-cyanide or diamond [Ref. 1: p. 36]. These flashes could be observed in a darkened room when viewed through a microscope of approximately thirty power. It was later determined that each scintillation corresponded to the impact of an individual alpha particle. Despite the physiological constraints limiting research to counting rates of approximately sixty scintillations per minute, many of the basic experiments of nuclear physics were performed using this technique.

The observation of alpha particles undergoing large angle scattering led to the demise of Thompson's model of the atom. Rutherford's subsequent theory of the nuclear atom and a revised prediction of alpha scattering received extensive testing in 1913 by Geiger and Marsden using a zinc sulfide screen which could be positioned at various angles around a foil target. Protons were detected by Rutherford in 1919 when he used a zinc sulfide screen to observe charged particles (the protons) which were created by the interaction

of alpha particles from radium C (bismuth 214) with nitrogen nuclei.

In 1944 Curran and Baker [Ref. 2: p. 1] introduced a simple version of the modern scintillator by replacing the human observer with a photomultiplier and registering the scintillation events on an electronic counting device. At a later time Kallman independently developed this same technique and applied it to the measurement of both quanta and particles. Kallman's subsequent discovery of energy proportionality in scintillation counting led to significant advances in determining the energy of radiations.

Since 1947 scintillation has been revived with the discovery of phosphor materials with sensitivity to beta and gamma radiations as well as heavy charged particles. The application of sodium iodide with a thallium activator for gamma detection was successfully pioneered by Robert Hofstadter and is now a standard scintillation material.

Although the human eye is no longer used to measure the twinkling effect of photons emerging from a fluorescent screen, the history of this technique is remembered through the application of the name scintillation to modern processes.

III. SCINTILLATION PHYSICS

A. PHOTON REACTIONS

The interaction of a photon with the medium through which it is passing is characterized by discrete reactions of three major types. These are the photoelectric, Compton and pair production processes. The photoelectric effect predominates for low energy photons (up to several hundred KeV) and the pair production process dominates above several MeV.

The absorption of photons in matter follows the equation

$$N = N_0 \exp(-\mu x)$$

where:

N = number of remaining photons,

N_0 = number of incident photons,

μ = linear absorption coefficient, and

x = thickness of absorber.

The linear absorption coefficient is the sum of contributions from the photoelectric, Compton and pair production processes

$$\mu = \mu_{photo} + \mu_{Compton} + \mu_{pair}$$

It can also be shown that the absorption coefficient is related to the cross section per atom, σ by

$$\mu = A \rho \sigma / M$$

where:

A = Avogadro's number,

ρ = density of absorber, and

M = molar mass absorber.

We will now discuss each of these mechanisms and its contribution to the total absorption coefficient.

1. Photoelectric Effect

In the photoelectric effect a photon will excite an atomic electron, transferring all of the photon energy to that electron. This electron then escapes from the atomic system, losing energy equivalent to the binding energy in the process

$$E_{electron} = E_{photon} - E_{binding}$$

As a consequence of liberating an electron from the inner shells of an atomic system, an unstable vacancy has been created. This vacancy can be shifted outward by rearrangement of the orbital electrons or by emission of an Auger electron. Eventually, a free electron will be captured to

fill the vacancy. These processes combine to result in the release of energy (either in the form of characteristic X-rays or as kinetic energy of the Auger electron) equivalent to the binding energy of the liberated orbital electron.

The probability for occurrence of the photoelectric effect (expressed as its cross section) is given by Enge [Ref. 3: p. 192] as

$$\sigma_{photo} = \frac{32\,\pi\,\sqrt{2}\,Z^5}{3\,(137)^4}\left(\frac{m_0\,c^2}{h\,\nu}\right)^{7/2} \qquad (1)$$

This expression is valid for photon energies in excess of the K shell binding energy. At these energy levels, about 80% of the total photoelectric absorption is due to the K shell [Ref. 4: p. 30]. As the photon energy approaches the rest energy of an electron, relativistic effects will cause the 7/2 exponent to decrease to 1, but the Z dependence is unchanged.

2. Compton Effect

In the Compton effect a photon of energy $h\nu$ strikes an electron, and is scattered off at an angle (θ) but at a reduced energy, $h\nu'$ (Figure 2)

$$h\nu' = \frac{h\,\nu}{1 + h\nu(1-\cos\theta)/m_0c^2} \qquad (2)$$

The energy of the recoiling electron is a function of the angle θ,

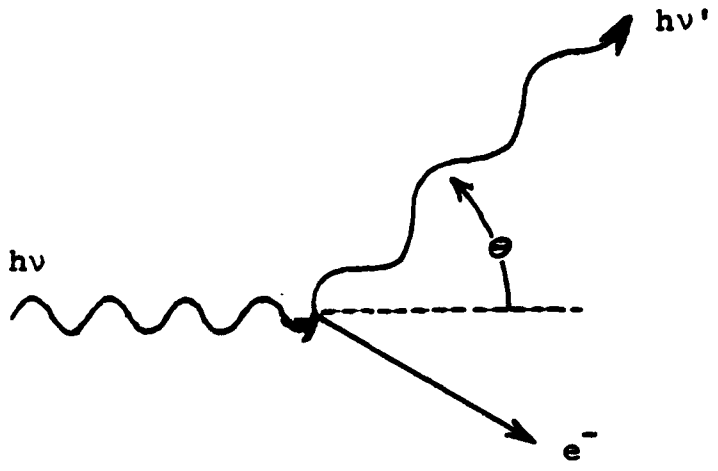

Figure 2. Compton Scattering

$$E_{electron} = h\nu - h\nu' = h\nu \frac{h\nu(1 - \cos\theta)/m_0c^2}{1 + h\nu(1 - \cos\theta)/m_0c^2}$$

This energy is a maximum for a head-on collision ($\theta = \pi$)

$$E_{electron_{max}} = h\nu \frac{2h\nu/m_0c^2}{1 + 2h\nu/m_0c^2} = \frac{3.914\ E_\gamma^2}{1 + 3.914\ E_\gamma}$$

where E_γ is the energy of the incident photon in MeV. Within a detector all scattering angles will occur, and a continuum of energies is produced. A sharp drop occurs at the maximum energy, and is known as the Compton edge.

In the above equations it was assumed that the electron was free and not bound to any atomic system. This is a valid assumption in most cases because the energy of the incident photon is very much greater than the electron binding energy. However, in real systems the electrons are bound and consequently the Compton edge will have a finite slope with a rounding off of the corners. The angular distribution of the scattered photons is predicted by the Klein-Nishina formula

$$\frac{d\sigma}{d\Omega} = r_0^2 \left[\frac{1}{1+\alpha(1-\cos\theta)}\right]^3 \left[\frac{1+\cos^2\theta}{2}\right] \left[1 + \frac{\alpha^2(1-\cos\theta)^2}{1+\cos^2\theta[1+\alpha(1-\cos\theta)]}\right]$$

where:

$\alpha = h\nu/m_0c^2$, and

r_0 = classical electron radius.

This relationship is represented graphically in Figure 3 which shows an increase in scatter in the forward direction with increasing photon energy.

The differential cross section can be integrated to yield the Compton scattering cross section per electron [Ref. 3: p. 192]

$$\sigma_{ce} = \frac{\pi}{\alpha}\left(\frac{e^2}{4\pi\varepsilon_0 m_0 c^2}\right)^2\left\{\left[1 - \frac{2(\alpha+1)}{\alpha^2}\right]\ln(2\alpha+1) + \frac{1}{2} + \frac{4}{\alpha} - \frac{1}{2(2\alpha+1)^2}\right\}$$

where:

$$\alpha = h\nu/m_0c^2.$$

The atomic cross section is the electronic cross section times the atomic number,

$$\sigma_c = \sigma_{ce} Z \qquad (3)$$

3. Pair Production Effect

Photons with high energy can convert that energy into an electron-positron pair when in an electric field. Energy in excess of the rest mass of the two particles (1.02 MeV) appears as kinetic energy of those particles. The cross section for pair production is [Ref. 3: p. 192]:

$$\sigma_{pair} = \frac{Z^2}{137}\left(\frac{e^2}{4\pi\varepsilon_0 m_0 c^2}\right)\left(\frac{28}{9}\ln\frac{2h\nu}{m_0c^2} - \frac{218}{27}\right).$$

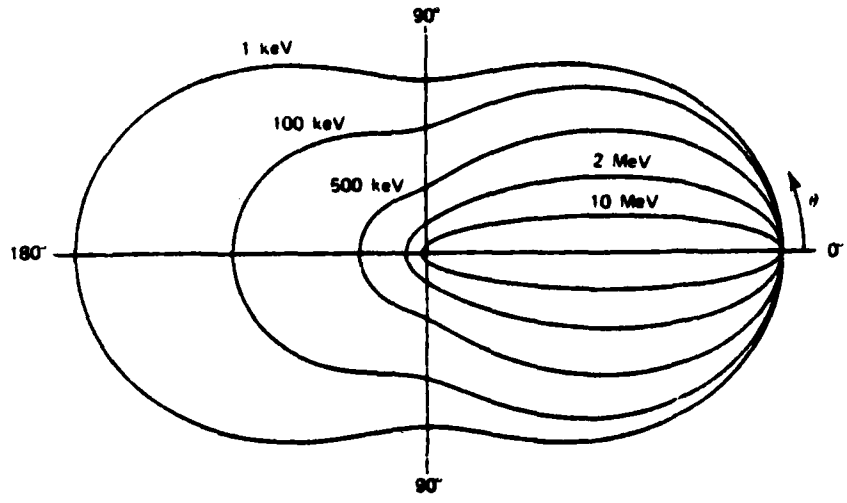

Figure 3. Angular Distribution of Scattered Photons as Predicted by Klein-Nishina Formula

B. SECONDARY ELECTRON ABSORPTION

Electrons (and positrons) dissipate their kinetic energy primarily through coulomb force interaction with the bound electrons of many atomic systems. Coulomb fields extend throughout the medium and subject the primary electron to continuous electromagnetic forces and lead to many excitation and ionization events which account for the loss of the electron or positron kinetic energy. This is in marked contrast to the rather discrete processes by which photons interact with matter. The rate of energy loss due to coulomb collisions is given by [Ref. 5: p. 56]:

$$-\left(\frac{dE}{dx}\right)_c = \frac{2\pi e^4 NZ}{m_0 v^2}\left\{\ln \frac{m_0 v^2 E}{2I^2(1-\beta^2)} - \ln 2\left(2\sqrt{1-\beta^2} - 1+\beta^2\right)\right.$$

$$\left. + (1-\beta^2) + \frac{1}{8}\left(1-\sqrt{1-\beta^2}\right)^2\right\}$$

where:

m_o = electron rest mass,

v = velocity of primary particle,

β = v/c

Z = atomic number of absorber atoms,

N = number density of absorber atoms,

I = average excitation and ionization potential of absorber,

E = energy of primary particle, and

e = electronic charge.

Because the primary electron has a mass equal to that of the target electron, large deflections in trajectory and large energy transfers can be achieved. The angular accelerations due to these deflections will result in radiative losses of energy by bremsstrahlung. The linear specific energy loss by bremsstrahlung radiation is [Ref. 5: p. 57]:

$$-\left(\frac{dE}{dx}\right)_r = \frac{N E Z(Z+1) e^4}{137 m_0^2 c^4}\left(4 \ln \frac{2E}{m_0 c^2} - \frac{4}{3}\right)$$

Losses due to radiation become dominant for large values of electron energy. The ratio of the radiation to collision loss rate is given by [Ref. 5: p. 57]:

$$\frac{(dE/dx)_r}{(dE/dx)_c} \simeq \frac{E Z}{700}$$

An additional factor to be considered for the energy deposition due to a positron is the annihilation reaction. Once the positron has been thermalized, it will react with an electron to release two photons of .511 MeV each.

C. SHOWER CASCADE

When an energetic photon interacts with matter, it will produce secondary electrons (and positrons) by photoelectric, Compton and pair production processes. These electrons will have a continuum of energies ranging up to the energy of the original photon. Bremsstahlung from these electrons will

cause more photoelectric, Compton, and possible pair production events, which in turn can generate more bremsstrahlung. In each subsequent generation of charged particles or bremsstrahlung, the individual energies are reduced until eventually the most energy intensive events can no longer occur. As photon energies decrease there will be a diminished yield of electron-positron pairs, then a reduction in Compton energies, until finally only photoelectric events occur. With a reduction in the energy of charged particles, there will be less bremsstrahlung formation and more ionization/ excitation along the particle track. Ultimately, the X-rays from ion recombination will only be able to cause excitation of atomic states, and these will decay by characteristic X-rays or by phonon emission.

This long chain of energy transitions between electromagnetic and kinetic energy is called the cascade shower.

D. DOPANT/ACTIVATOR

The molecules of inorganic scintillation materials form a crystal lattice and determine energy bands in which excited electrons may exist. For most materials, the band gap between the valence and conduction bands corresponds to energy transitions beyond the visible spectrum. The addition of an impurity dopant to a pure crystal can create activator ground and excited states within the "forbidden" band. An electron in one of these intermediate energy positions can de-excite to the valence band, releasing less than the full band gap energy.

With judicious choice of a dopant (activator), a transition can be obtained which results in the emission of a photon of visible light.

A typical scenario for the conversion of an incident radiation to visible photons is as follows:

passage of a charged particle creates electron-hole pairs;

a hole drifts to an activator location and ionizes it;

an electron migrates to the ionized activator and excites it;

the excited activator emits a visible photon after a decay time on the order of 10^{-8} seconds (the electron migration time is much shorter than the decay time).

The emitted photon has insufficient energy to create additional electron-hole pairs, and so it will propagate through the crystal until it leaves the physical confines of the scintillator.

Once the primary radiation has been broken down into visible photons of a characteristic energy, those photons must be removed from the scintillator and counted. However, problems arise during the propagation through the scintillating material to the exit window. Since the photons were emitted by an atomic transition, they are at the right resonant frequency to cause the reverse transition and raise like atoms to an excited state. The newly excited atom may decay by release of another photon but there is also a distinct possibility for non-radiative decay by phonon emission. A long chain of absorption-emission sequences will reduce the photon

intensity due to the cumulative losses of phonon decay, and will also lengthen the time duration of the photon shower from the primary event. If the showers from separate initial events begin to overlap, one has lost the ability to associate scintillation photons with a particular incident radiation and subsequently the energy of that radiation cannot be determined.

By restricting the activator population to a small concentration, the problem of re-absorption of the visible scintillation can be minimized. Sodium iodide (NaI) is a very common scintillation crystal and typically has an activator concentration of 10^{-3} mole fraction thallium [Ref. 4: p. 259].

E. COUPLING SURFACES AND REFLECTORS

A scintillator will usually be connected to a photodetection device on only a portion of the total scintillator surface. Steps must be taken to maximize the coupling of photons through this interface, and also to minimize the loss of photons through the remainder of the scintillator geometry.

A difference in refractive indices will result in a refraction of the optical path in accordance with Snell's Law:

$$n_1 \sin \theta_1 = n_2 \sin \theta_2$$

Beyond a critical angle, θ_c, refraction is no longer possible and total internal reflection occurs.

$$\theta_c = \sin^{-1} \frac{n_2}{n_1}$$

The index of refraction for most scintillators is in the range of 1.5 to 2.3, and the glass face of photo-multiplier tubes is typically 1.5. Any gap of air (n = 1) in the scintillator-photomultiplier tube interface can result in a severe mismatch of indices, and limit the cone of escaping photons to a small angle. The air gap is precluded by applying a coupling film of optical grease or oil (n ~ 1.5) to cover any irregularities on the interface. If photons can be reflected back into the crystal from free surfaces, they will propagate within the crystal, hopefully reach the phototube interface and have an additional chance to penetrate into the phototube. Two types of reflectors are available for this purpose. A specular reflector, such as a polished metal like aluminum foil, creates a situation where the angle of incidence is equal to the angle of reflection. A diffuse reflector, e.g., a coating of magnesium oxide powder, produces a condition where the angle of reflection is fairly independent of the angle of incidence. The diffuse distribution is given by Lambert's Law:

$$\frac{dI(\psi)}{dI_0} = \cos \psi$$

where ψ is the reflection angle with respect to the surface normal.

IV. BGO AS A SCINTILLATOR

Bismuth Germanium Oxide ($Bi_4Ge_3O_{12}$) is a relatively new scintillator material, which because of the high atomic number of its components and a high density make it spatially efficient for the capture of high energy radiations. The mechanical and chemical stability of this bismuth germanate (BGO) enable it to be handled and machined far more easily than many other scintillator materials. Table I summarizes many physical characteristics of BGO relative to sodium iodide.

Crystals of BGO are grown from a stoichiometric melt of pure bismuth oxide (Bi_2O_3) and germanium oxide (GeO_2), using the Czochralski method. Pulling rates are 3-4 mm per hour at 20 rpm. The resulting boule has a cubic "eulytine" structure which can be formed into desired shapes by conventional machining and polishing techniques.

The biggest physical disadvantage of bismuth germanate is in its high index of refraction (n = 2.13) which inhibits the coupling of scintillations from the crystal into photomultiplier tubes which typically have glass windows with index 1.5. This reduced light output drops the pulse height from a BGO coupled photomultiplier tube to only 8-16% [Ref. 6] of that from a sodium iodide scintillator.

The fluorescent spectral response of scintillations created in BGO is depicted in Figure 4 [Ref. 7: p. 5497]. This luminescence has been attributed [Ref. 7: p. 5495] to

TABLE I

Physical Properties of Bismuth Germanate and Thallium Activated Sodium Iodide

		BGO	NaI(Tl)
Mechanical:			
	Density	7.13	3.67
	Hardness	5	2
	Stability	rugged	easily cleaved shattered
Chemical:			
	Solubility (water)	none	very hydroscopic
	Refractive Index (visible light)	2.13	1.85
Scintillation:			
	Wavelength of Max. Intensity	480 nm	420 nm
	Decay Constant	.30 sec	.25 sec
	Rise, Fall Times	50, 300 nsec	50, 250 nsec
	Resolution		
	Cs-127 (.66 MeV)	15%	7%
	Na-22 (.511 MeV)	16%	
	(1.27 MeV)	11%	
	Relative Pulse Height	8	100

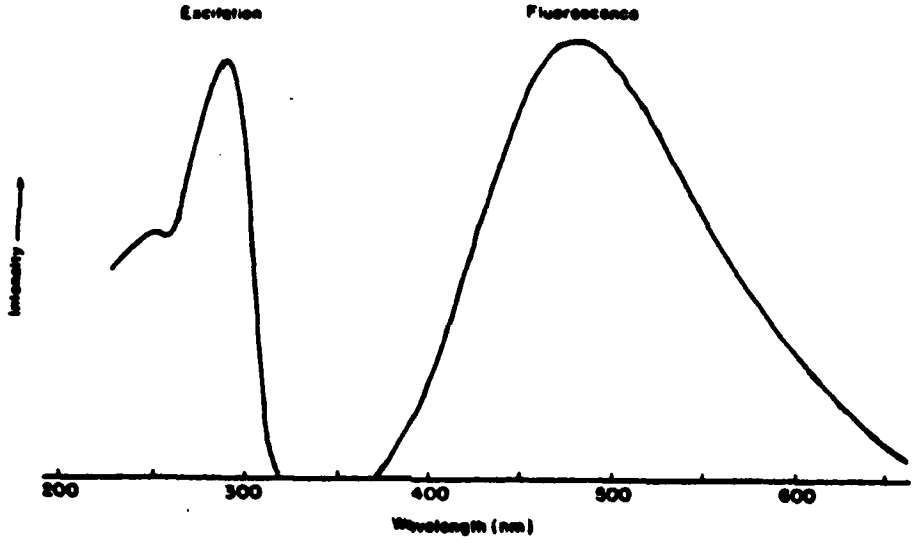

Figure 4. Excitation and Fluorescent Spectral Response of Bismuth Germanate

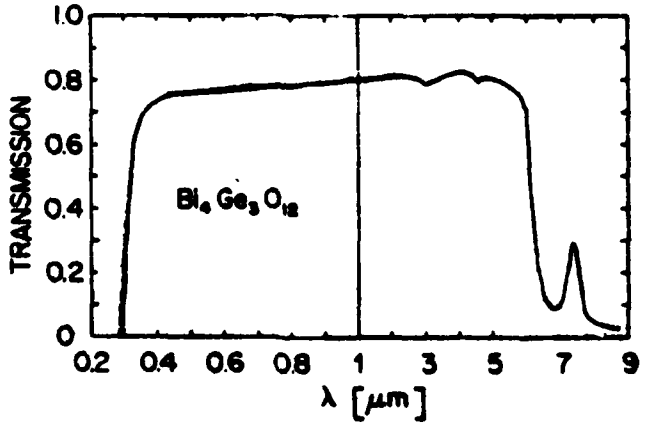

Figure 5. Optical Transmission of Bismuth Germanate

the $^3P_1 \rightarrow {}^1S_0$ electronic transition of Bi^{+3} ions. Trivalent bismuth ions have a mercury-like $6S^2$ electronic configuration and a $^1S_0$ ground state. The lowest excited states of Bi^{+3} are $^3P_0$, $^3P_1$, $^3P_2$, and $^1P_1$. Of these, the $^3P_0$ and $^3P_2$ states are forbidden for optical excitation from the ground state. (J can not go from 0 to 0, and ΔJ can not be 2.) Absorption peaks for the excitation to the $^3P_1$ and $^1P_1$ states are at 290 and 250 nanometers respectively. These two peaks constitute the "300nm absorption edge" of the optical transmission curve (Figure 5) [Ref. 8: p. 5110].

Upon excitation, there is a large Stokes shift of about $14{,}000cm^{-1}$ [Ref. 7: p. 5498] wherein electronic energy is shifted into rotational/vibrational energy of the molecule. Consequently, when the $^3P_1$ state relaxes to the ground state via photon emission, that photon will have less energy than was required for the original excitation. The excitation and fluorescent spectra do not overlap. For this reason, bismuth germanate is quite transparent to scintillation photons and no activator material is required.

V. PHOTOMULTIPLIER TUBE CHARACTERISTICS

A photomultiplier tube functions to measure a photon flux by converting photons into low energy electrons at the photocathode and then amplifying these photoelectrons into a current which can be used by a follow-on device, such as a pulse height analyzer.

A. PHOTON CONVERSION

The photo-emission from the photocathode is the culmination of three steps wherein the photon is absorbed transferring its energy to electrons of the photo-emissive material; the electrons migrate to the surface; and finally, the electrons escape from the surface [Ref. 5: p. 272-284].

Photons typical of scintillator outputs have energies of about three electron volts. Some of this energy will be lost in collisions prior to reaching the photocathode. Once absorbed in the photocathode, the photon must release an energy at least equal to the work function (the potential barrier at the interface of material and a vacuum) in order to cause the emission of an electron. Most metals have a work function of 3 to 4 ev, but values as low as 1.5 to 2 ev are obtainable for specially prepared semiconductors. The work function imposes a minimum energy level for photons to produce free electrons; this energy cutoff usually corresponds to light in the red or the infra-red frequencies.

The escape depth is that depth within a material from which an electron can originate and still have an energy in excess of the work function by the time it has migrated to the surface. Because electrons lose energy very quickly during passage through metals, they can traverse only a few nanometers before their energy is reduced below the critical energy level. Semiconductors are less efficient in stopping electrons and can have an escape depth as great as twenty-five nanometers. These distances are small relative to that required to stop visible light; as a result, less than half of the incident light interacts within the photosensitive layer.

To produce photoelectrons in semiconductor materials, the photon must have an energy greater than the bandgap energy in order to cause excitations from the valence band to the conduction band. As a result of phonon interactions with the crystal, the electron will lose energy and drop to the bottom of the conduction band after one picosecond of excitation. The excited electron has a lifetime of one hundred picoseconds before recombination with a hole and subsequent return to the valence band. The work function is usually higher than the energy level at the bottom of the conduction band, so the electron must reach the surface of the photoemissive material within that one picosecond after excitation. However, some semiconductors have been developed which have a negative electron affinity and electrons can escape from the surface

even if at the bottom of the conduction band. Negative electron affinity materials have a much greater migration time available, and therefore a much greater escape depth.

Thermionic noise is the spontaneous emission of electrons from a surface due to electrons attaining a high energy within the thermal kinetic energy distribution and exceeding the work function. At room temperature metals have approximately one hundred thermal emission electrons per square meter per second, whereas semiconductors experience a thermionic loss at a rate of 10^6 to 10^8 per square meter per second. Semiconductors have a greater sensitivity to incident photons but also have a greater noise problem.

Photocathodes are of two physically different types. The semi-transparent photocathode is usually no thicker than the escape depth and the electrons are collected from the surface opposite to the incident photon flux. The photoemissive material is deposited on a transparent backing, such as the glass end window of the photomultiplier tube. For the opaque type photocathode, the material is slightly thicker than the escape depth and is supported by a thick backing. Electrons are collected from the incident surface.

The quantum efficiency of a photocathode is defined as the number of photoelectrons produced per incident photon. Practical photomultiplier tubes have a maximum quantum efficiency of twenty to thirty percent. This parameter will be a function of the quantum energy of the incident light.

Therefore it is essential to match the scintillator emission spectrum with the photocathode spectral sensitivity.

Photocathodes are subject to constraints on the range of photon frequencies to which they can be coupled. A low frequency limit is dictated by the requirement that the photons have sufficient energy to interact with the photocathode and produce energetic electrons which can migrate to the surface and escape. Upper frequency limits are imposed by the glass envelope of the photomultiplier tube which will absorb photons with a wavelength less than 350 nm. By use of fused silica or quartz windows, this limit can be extended to a corresponding wavelength of approximately 160 nm.

B. ELECTRON AMPLIFICATION

Electrons leave the photocathode with an energy of about one electron volt and are accelerated by a positive electric potential along a path whereby the electron collides with an electrode (called a dynode) causing excitation of many electrons within that dynode. For a dynode bandgap of two electron volts, an accelerating potential of one hundred volts can theoretically produce up to fifty secondary electrons. However, due to the random direction of these excited electrons, few will reach the surface with sufficient energy to escape. The multiplication factor for a single dynode is defined as:

$$\delta = \frac{\text{NUMBER OF EMITTED SECONDARY ELECTRONS}}{\text{NUMBER OF PRIMARY INCIDENT ELECTRONS}} .$$

The energy of the incident electron is a factor in determining the secondary electron yield. An incident electron of low energy will excite only a few dynode electrons, but the interaction will be close to the surface so escape is likely. For high energy incidence, many excitations will occur, albeit at a greater depth which reduces the probability of escape. An optimum incident energy does exist between these extremes, and is of importance in determining the voltage separation between successive dynodes in a cascaded amplification process. Figure 6 [Ref. 5: p. 279] depicts the effect of primary electron energy on the secondary emission gain for various dynode materials. Although a multiplication factor approaching ten is possible for a single dynode operating at an optimum potential of one KeV, actual operation of cascaded dynode tubes involves interstage voltages of a few hundred volts and a gain of four to six per stage.

The overall gain is given by

$$\alpha\delta N$$

where:

α = fraction of all photoelectrons collected by the multiplier structure;

δ = secondary emission gain per stage;

N = number of stages.

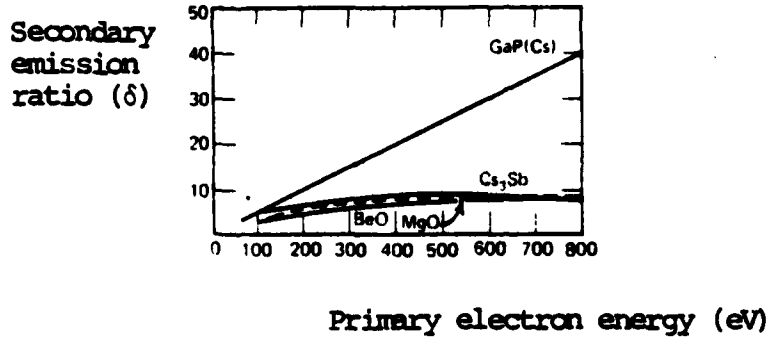

Figure 6. Secondary Emission Gain as a Function of Incident Electron Energy for Various Dynode Materials

For a ten stage photomultiplier operating with total collection and a δ of 5, the gain will be approximately 10^7.

The emission of secondary electrons is a statistical process and the gain at a given dynode will vary from event to event. The Poisson process is often used as the simplest model of dynode amplification. In this case the number of secondary electrons will have a mean value of δ and a standard deviation of $\sqrt{\delta}$. The relative variance is

$$\left(\frac{\sigma}{\delta}\right)^2 = \frac{1}{\delta}$$

and when compounded over N stages it becomes

$$\frac{1}{\delta} + \frac{1}{\delta^2} + \ldots + \frac{1}{\delta^N} \simeq \frac{1}{\delta - 1}$$

When the gain δ is much greater than one, the relative variance or spread in output pulse amplitude is dominated by fluctuations in yield from the first dynode where the number of electrons is lowest. Although more detailed studies of photomultiplier statistics [Ref. 9: pp. 161-175; Ref. 5: pp. 89-92] modify the Poisson assumption, all agree on performance being limited by the stage with minimum input. The greatest fluctuations occur when poor light collection or low energy radiations are involved.

Remembering that BGO has a scintillation output which is only 8% relative to sodium iodide, it can be expected on

purely statistical grounds that BGO analysis will have greater fluctuations and a poorer energy resolution.

In a study of the statistical theory of noise in photomultiplier tubes by RCA [Ref. 9: p. 174] an expression for the energy resolution full width at half maximum (FWHM) is developed wherein:

$$\text{FWHM} = 2.355 \left[\frac{1 - \eta + \frac{1}{\delta - 1}}{m_c \, \eta} + \frac{\sigma_c^2}{m_c^2} \right]^{1/2}$$

where:

η = photocathode quantum efficiency,

δ = secondary emission gain per stage,

m_c = number of scintillation photons corresponding to the photopeak,

σ_c^2 = variance in number of photons per photopeak pulse.

The first expression within the radical is the photomultiplier contribution to the relative variance and the second term reflects the FWHM due to crystal statistics alone. Since it is desirable to have a small FWHM, it can be seen that a reduced photon output η will adversely affect the resolution from both sources.

VI. PULSE HEIGHT ANALYSIS

Once incident nuclear radiation has been converted to visible photons by the scintillator and then into an electrical signal by the photomultiplier tube, that signal can be amplified further by electronic means and accumulated into a pulse heat analyzer (PHA).

An analog to digital converter within the PHA breaks the input signal down into sequential intervals of voltage values. Each input pulse is then directed to a memory location corresponding to that particular voltage, and the number stored in that memory (channel) is incremented by one. After a period of accumulating the input signal, the PHA display will graphically depict the frequency occurrence for each voltage interval. A sample spectrum representing the radiation from cesium-137 is shown in Figure 7. The absorption of all energy via the photoelectric effect results in a signal being transferred to the PHA which corresponds to the full energy of the original radiation and is displayed as a "photopeak". Ideally, this peak should be a single vertical line, but in reality it is subject to statistical broadening as discussed previously.

When many absorption processes are involved in transforming the radiation into scintillation photons, yet the cascade shower is still completely contained within the crystal, then a signal voltage representing the full energy is again sent

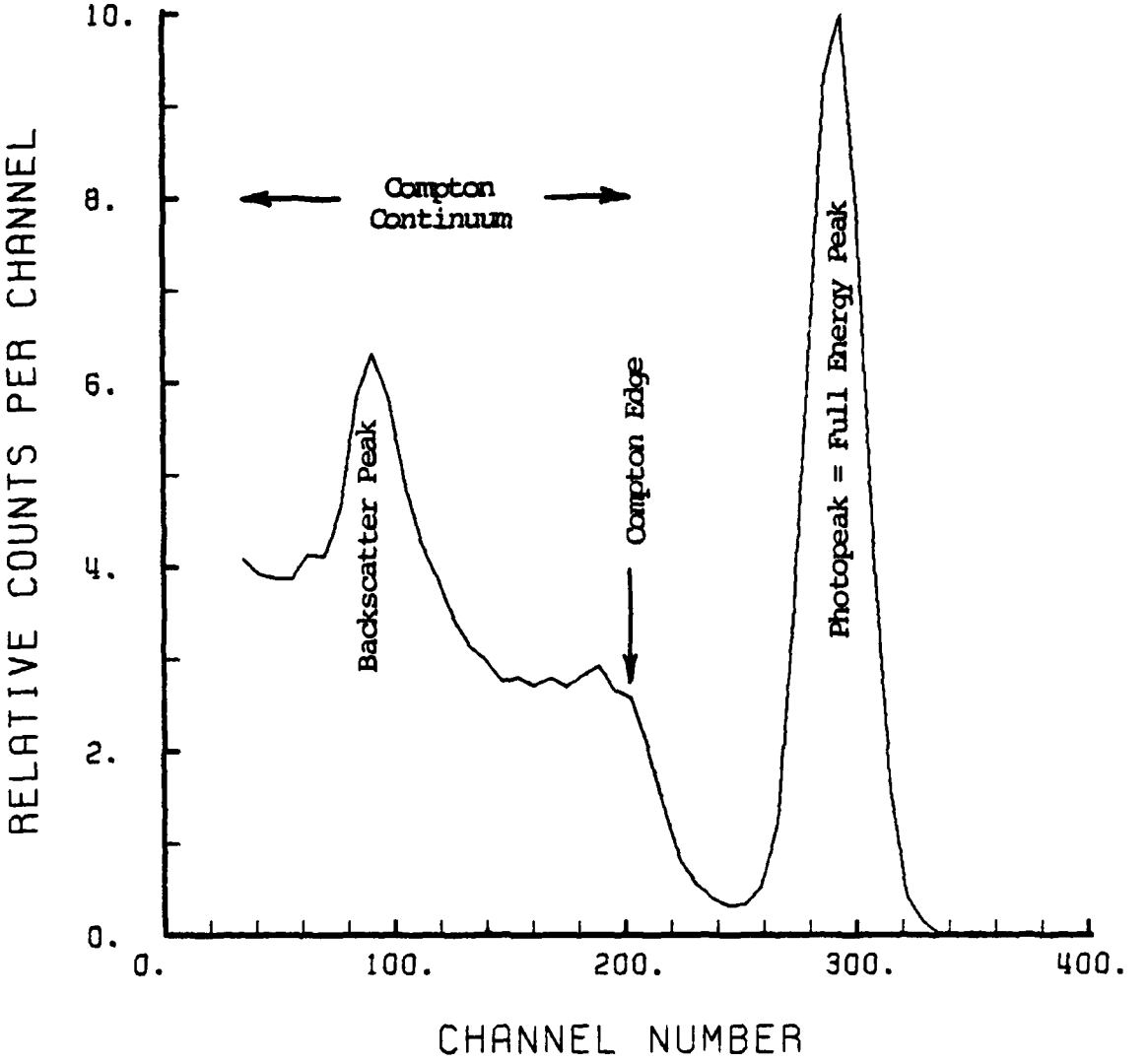

Figure 7. Pulse Height Spectrum of Cesium-137 Using a NaI(Tl) Scintillator

to the PHA. For this reason the photopeak is sometimes referred to as the full-energy peak.

If all steps in the transformation of the incident radiation into the final scintillations of visible light are performed via radiative transitions and captured within the crystal, then all the initial energy is accounted for in the scintillations. This means that the signal leaving the scintillator crystal is proportional to the energy of the original radiation. The signal losses at the interface to the photomultiplier tube are due to statistical processes and do not change the proportionality concept. Amplification within the phototube will depend on the scintillation photon energies, but since these are independent (in energy although not in number) of the original radiation, the proportionality is preserved. A threat to proportionality exists from the non-radiative losses experienced within the scintillator crystal. Phonon losses can be minimized by operating the system at reduced temperatures; usually room temperature is acceptable but elevated temperatures should be avoided. Additionally, if the crystal is designed so that the non-radiative losses occur predominantly at energies less than the lowest incident energy to be measured, then these losses have a similar effect on the showers from all incident radiations and proportionality is still maintained. The premise of proportionality is paramount to pulse height analysis as this enable the PHA channel numbers, which are a measure of pulse strength, to be linearly

expressed in terms of the energy of the primary radiation being detected.

The absorption of energy by Compton processes introduces the possibility that the recoiling photon may escape from the crystal prior to total absorption. For a Compton event with maximum energy transfer to the electron, a recoil photon is created with energy

$$E_{\gamma'_{min}} = E_\gamma/(1 + 4E_\gamma) \qquad \text{(Eq. 2 with } \theta = \pi\text{)}$$

The escape of this recoil photon results in decreased energy being transferred to the PHA, and is registered to the left of the photopeak by an amount equivalent to $E_{\gamma'_{min}}$. Other Compton collisions create photon sequences with energies between $E_{\gamma'_{min}}$ and E_γ; their loss results in a continuum of events to the left of the minimum Compton loss. The upper limit on the Compton continuum is referred to as the Compton edge and has a value of

$$E_{\text{Compton edge}} = E_\gamma - \frac{E_\gamma}{1 + 4E_\gamma} = \frac{4\,E_\gamma^2}{1 + 4E_\gamma}$$

The previous discussion of Compton losses has assumed that the incident radiation produced only one Compton event prior to photoelectric absorption. Cascade showers with multiple Compton scattering will produce recoil photons of progressively lower energy. Loss of these low energy photons

will tend to fill in the gap between the photopeak and the Compton edge. Additionally, the escape of any secondary electron prior to the complete absorption of its kinetic energy will result in events which are offset from the photopeak by the amount of lost kinetic energy.

Backscatter peaks are the result of interaction between the radiation source and shielding materials adjacent to the scintillation crystal (Figure 8) [Ref. 10: p. 17]. Radiation from the source produces Compton scattering in the shield and the recoiling photons can be absorbed by the scintillator with subsequent registration by the PHA. The backscatter not only produces a "false peak" which is not necessarily part of the source spectrum, but it also contributes a significant amount of counts which may mask desired peaks.

An escape peak is an accumulation of events where the detected energy is less than the photopeak energy by an amount corresponding to the loss of either a K shell X-ray or a positron-electron annihilation gamma ray. A double escape peak refers to a peak which is offset from the photopeak by 1.02 MeV, thus representing the escape of both gammas from an annihilation reaction. For scintillation crystals with a sufficiently large volume to surface area ratio, most X-rays will be absorbed prior to reaching the crystal surface; and X-ray escape peaks become insignificant.

In the analysis of radiation by the spectra created in pulse height analyzers, it is the photopeaks which provide

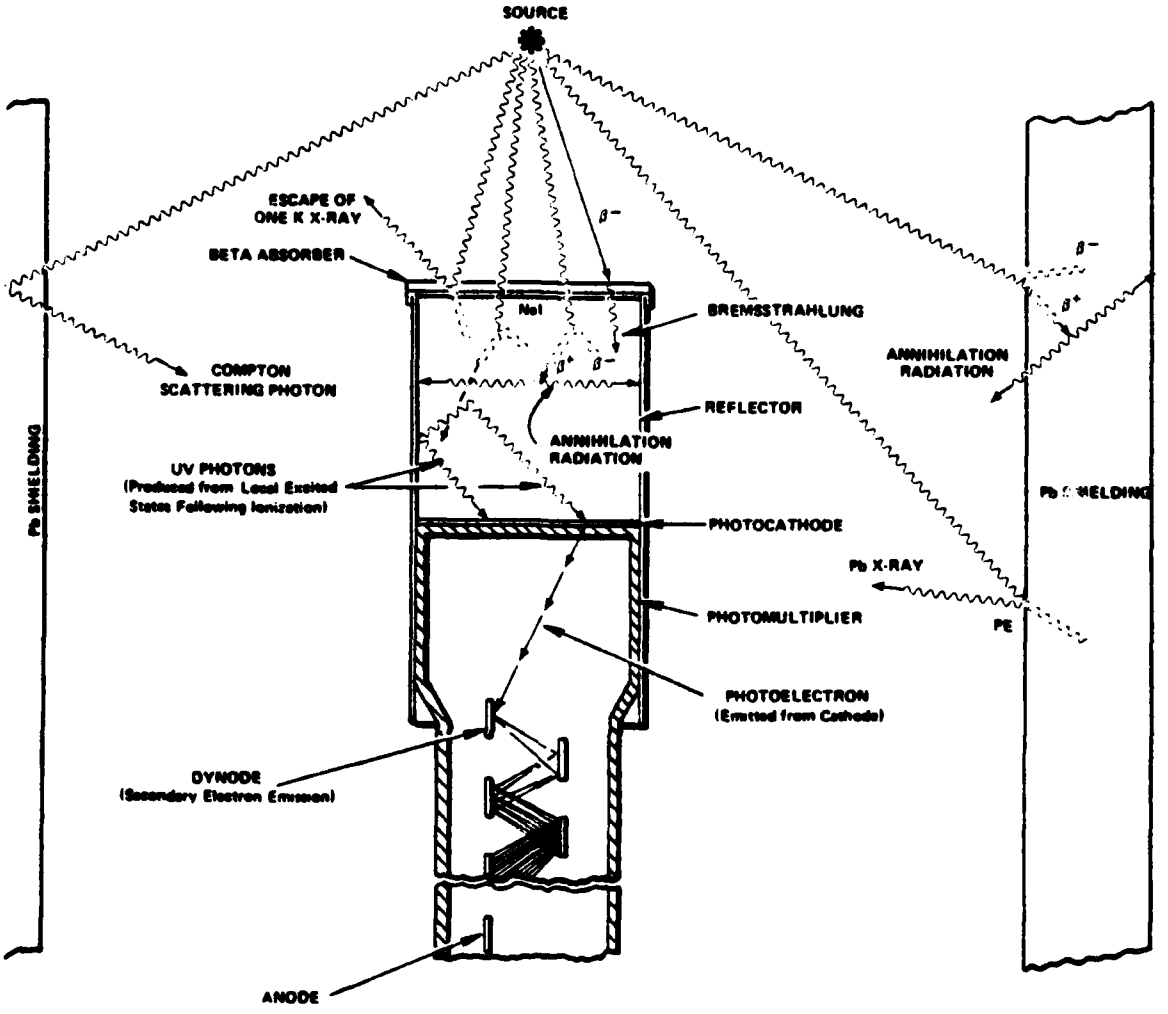

Figure 8. Geometry of a Typical Scintillation Counting Apparatus

information on the total energy of the incident radiations. The energy of the primary radiation is evaluated as that energy corresponding to the maximum of the photopeak. The narrower the photopeak is, the greater is the accuracy to which the energy can be ascertained and the less to which this peak will interfere with the evaluation of adjacent peaks. A quantification of this uncertainty in determining the peak energy value is provided by the resolution of the scintillation apparatus at the energy of interest. The resolution in percent is defined as the full width of the photopeak, measured at one-half of the maximum count level (FWHM), divided by the value of the centroid of the photopeak. Since the channel numbers of the PHA are proportional to the energy, the FWHM and centroid values can be expressed in terms of either parameter.

The continuum of Compton scattering events does not contribute toward determining the energy values, and has the adverse effect of burying any photopeaks from lower energy radiations which may fall within the Compton range. It is therefore desirable to maximize the contribution of photoelectric events relative to the Compton process. A comparison of the equations (1 and 3) which describe the probabilities for production of these two processes, indicates that the photoelectric cross section is proportional to the fifth power of atomic number Z, whereas the Compton cross section is proportional to Z in only the first power. The increase in

atomic number of BGO over NaI(Tl) should result in a much higher photopeak to Compton ratio for the bismuth germanate. This was experimentally verified and is readily apparent from the resolution spectra of cesium-137, sodium-22 and cobalt-60 (Figure 9) for these two scintillator materials.

Although the lower signal output of BGO results in poorer resolution of the photopeaks, it can be appreciated that the smaller Compton component in the BGO spectra will make it easier for the low energy photopeaks of a mixed radiation source to be detected above this Compton "noise".

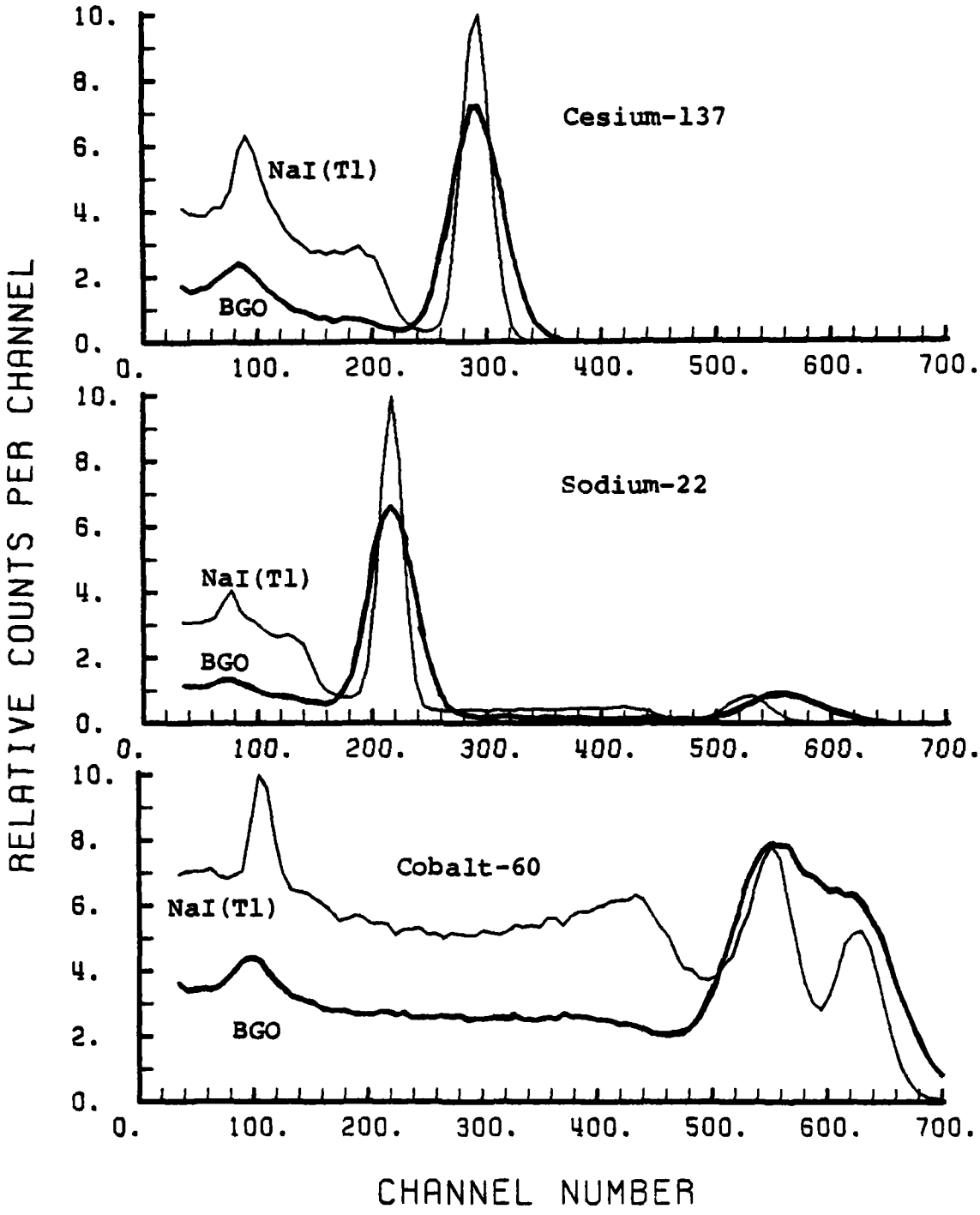

Figure 9. Comparison of BGO and NaI(Tl) Spectra of Cesium-137, Sodium-22 and Cobalt-60

VII. EXPERIMENTAL OBSERVATIONS

A. EQUIPMENT USED

Scintillation crystals of both BGO and of NaI(Tl) were analyzed by mounting them to a Hamamatsu type R329 photomultiplier tube, amplifying that signal electronically in an Ortec model 485 amplifier and displaying the results on a Tracor-Northern model TN-7200 Multichannel Analyzer. The photomultiplier tube was operated in a light-tight enclosure at an 1800 volt potential provided from a Hewlett-Packard/ Harrison model 6522A DC power supply. A Hewlett-Packard 3450A multifunction meter monitored the high voltage output (via a locally fabricated 100:1 voltage divider network) with feedback adjustment provided by operator personnel. Observation of the electrical signal from the photomultiplier tube, as well as from the Ortec amplifier was performed with a Tektronic type 454 oscilloscope. Finally, a record copy of the pulse height spectra was provided on an Epson model MX-100 terminal printer. This equipment setup is shown schematically in Figure 10 and by a photograph in Figure 11.

The crystal of bismuth germanate was acquired from the Harshaw Chemical Company as a cylinder of one inch height by one inch diameter with polished flat end windows and frosted cylindrical surfaces. Comparisons were made on the performance of this BGO to a type 6D4 sodium iodide (thallium) scintillator assembly from the same manufacturer. The sodium iodide

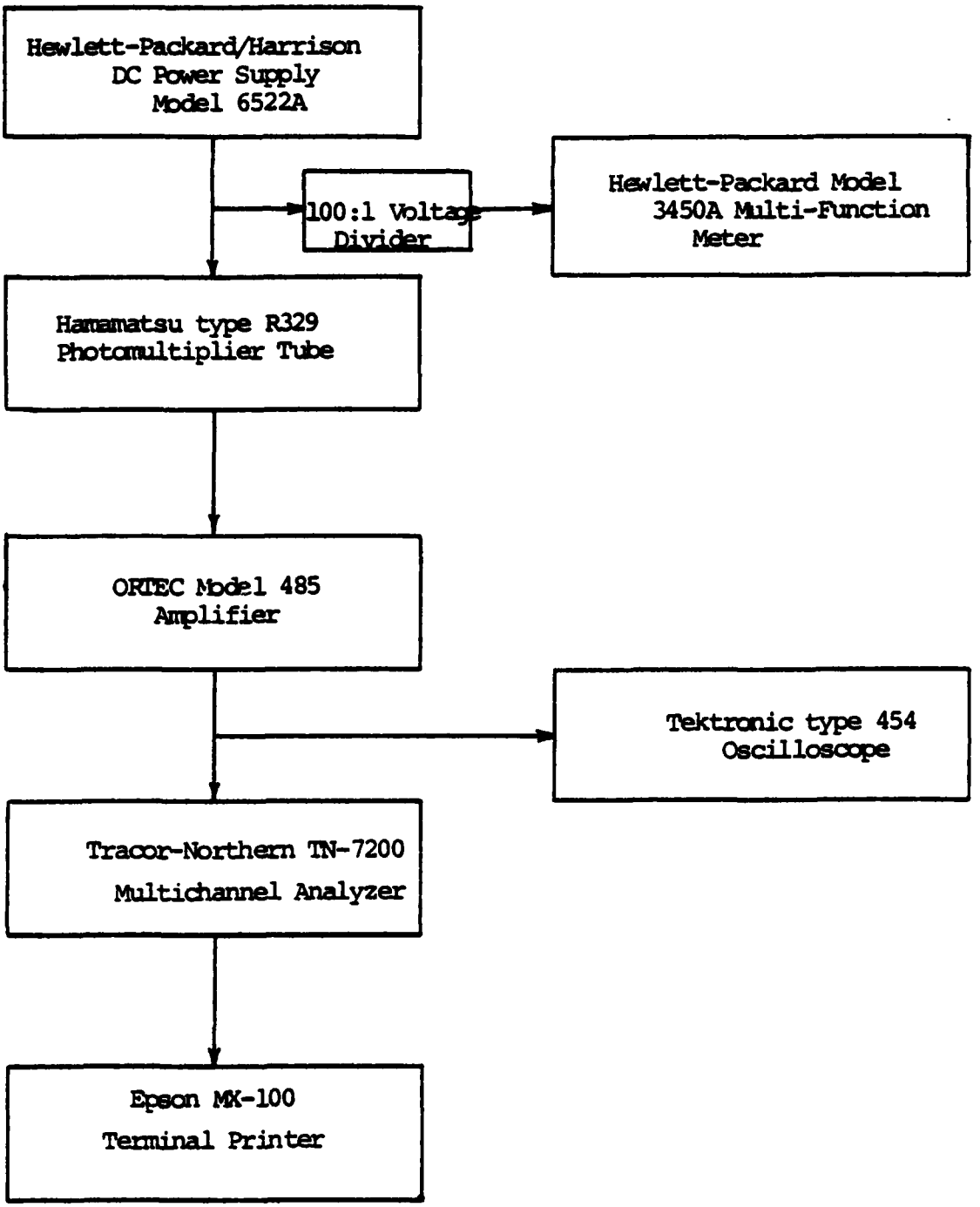

Figure 10. Block Diagram of Experiment Instrumentation

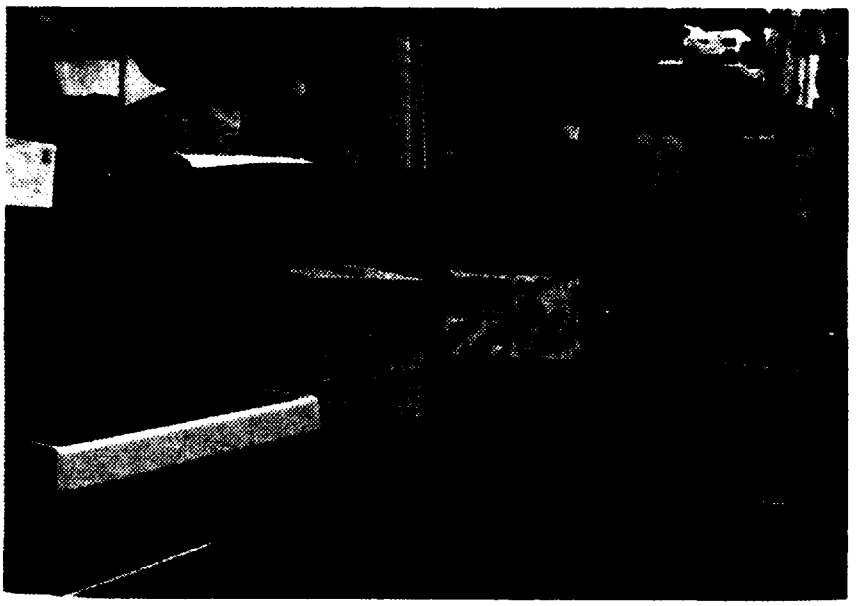

Figure 11. Photograph of Experiment Instrumentation

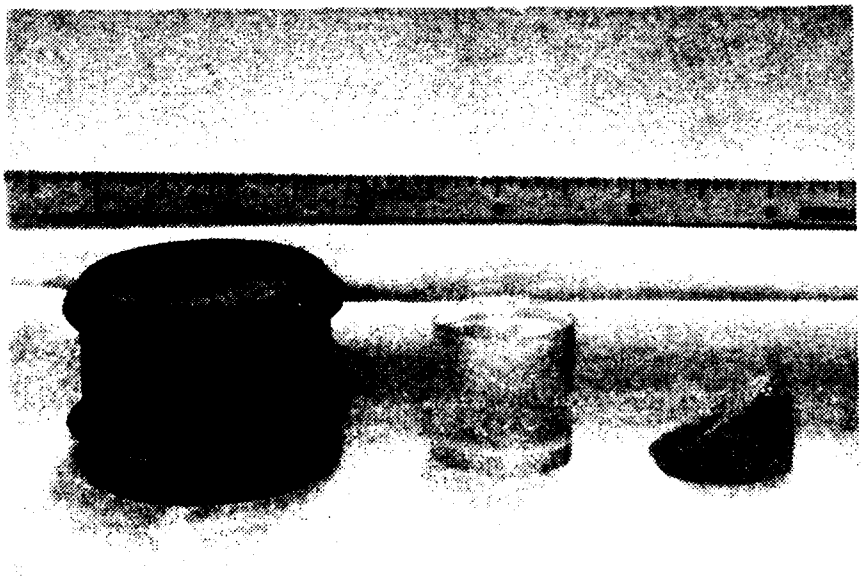

Figure 12. Photograph of NaI(Tl) and BGO Scintillation Crystals

scintillator consisted of a 1.5 inch diameter by 1 inch high NaI crystal, a 1/8 inch thick glass window, 1/16 inch of aluminum oxide packing and an aluminum enclosure.

After preliminary analysis with the BGO crystal, an unanticipated experiment in stress analysis provided the study group with many fragments of BGO when the original crystal was dropped onto a concrete floor. Two larger fragments each had an undamaged end window and were used with unexpected success in subsequent experiments. Figure 12 is a photograph of the fragment used in radiation damage studies, the sodium iodide assembly and a replacement BGO crystal of original size.

B. EFFORTS TO IMPROVE THE RESOLUTION OF BGO

In order to make any valid comparisons on the utility of BGO versus NaI(Tl) detectors, one must "package" the BGO in such a manner that it can compete with the NaI(Tl) which is usually supplied by its manufacturer as a sealed unit with an optimized reflector arrangement. Because bismuth germanate has a scintillation light output which is only eight percent relative to sodium iodide, every technique must be used to make the best use of what is available.

At the scintillator-photomultiplier tube interface a coupling problem arises due to a disparity in refractive indices between the glass (n = 1.5) and the scintillator material (n = 2.13 for BGO, n = 1.85 for NaI(Tl)). Any pockets of air (n = 1) at this interface, will seriously

aggravate an already critical problem. A thin coating of optical grease (oil) with an appropriate refractive index will eliminate the air and create a more uniform transition of refractive indices. Cargille's type B immersion oil ($n = 1.515$) was used in this study. The effectiveness of this coupling is demonstrated (by a NaI crystal) in Figure 13 which overlays two spectra of cobalt-60, the upper with and the lower without the optical coupling oil.

The power supply voltage level being fed to the photomultiplier tube was evaluated for possible effects on resolution by operating the photomultiplier tube at various base potentials from 1500 to 2000 volts and adjusting the electronic amplifier gain to provide a constant signal strength to the pulse height analyzer. The relatively constant resolution of the .511 MeV peak from sodium-22 indicated an independence of voltage level within this range. A value of 1800 volts was arbitrarily chosen as a standard operating condition for subsequent tests.

Given a fixed voltage supply, variations in electronic amplification techniques were studied for possible effects on resolution. Previous measurements [Ref. 6: p. 347] on BGO have used an RC integrator. An Ortec model 410 amplifier was used to obtain various rates of integration (as well as differentiation) for both unipolar and bipolar modes to determine the effectiveness of this technique.

Figure 13. Effect of Optical Coupling Oil on the Resolution of Cobalt-60 by a NaI(Tl) Scintillator

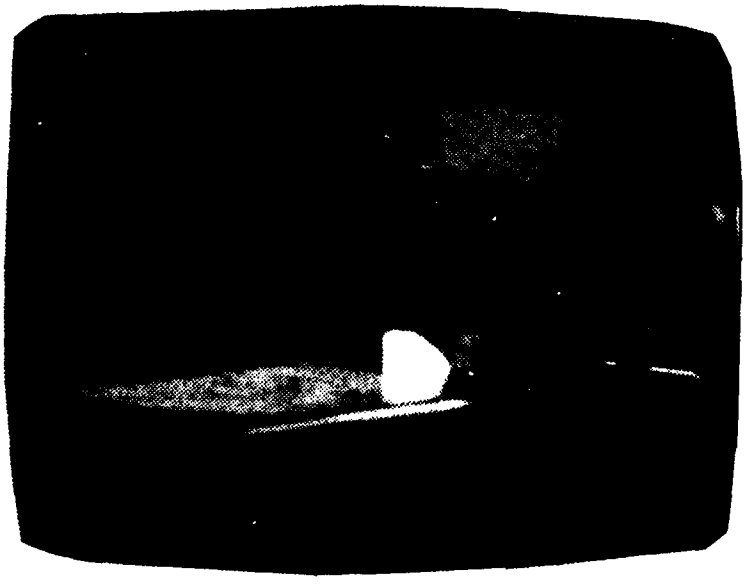

Figure 14. Illumination from Bismuth Germanate During Exposure to a 100 MeV Electron Beam

With the BGO crystal (vice NaI(Tl)) coupled to the photomultiplier tube, the tube's output was too low to drive the Ortec 410, so an Ortec 485 amplifier was used as an intermediate amplifier. No improvement in resolution was observed at any combination of control settings over the resolution which was obtainable by using the model 485 to feed the pulse height analyzer directly. Consequently, further tests used the Ortec 485 (set for negative input pulses and unipolar mode) as the sole electronic amplifier.

Having standardized the amplification portion of the BGO scintillation system, further refinements were then made to the scintillation crystal proper. By applying a reflective coating to the scintillator, the number of photons which escape through the coated surfaces was reduced. When these photons are reflected back into the crystal, the remainder of their energies can be absorbed in the crystal, thereby allowing all of the radiation's original energy to be converted to scintillation and contribute to the total energy peak rather than to the Compton continuum. Once photons have been reduced in energy to the scintillation level, the reflector causes them to bounce around inside the crystal until they can escape from the end window into the photomultiplier tube. A greater number of scintillations being transferred to the photomultiplier tube results in a better resolution, as was seen in the previous discussion of counting statistics.

In searching for an optimal reflector arrangement, many diffuse and specular coatings were evaluated. For a

monoenergetic source of incident radiation, the pulse height (voltage) of the amplified signal is a direct indication of the number of scintillations being coupled into the photomultiplier tube. This pulse height could be easily measured and was used as a figure of merit in comparing the effectiveness of various reflectors. (A higher pulse height represents a better reflector performance.) Table II summarizes the results of this testing and makes a comparison to the signal output from a NaI(Tl) assembly for the same aplifier gain. The ratio of the best BGO signal to that of the oil coupled sodium iodide assembly is 9.2%. Although the two scintillators are of different size, each is large enough to contain the electromagnetic shower at this energy level. This ratio of signal strengths is in close agreement with the previously cited 8% relative light output.

The best reflector performance for the BGO crystal was obtained by wrapping it in aluminum foil with the specular surface in contact with the BGO.

Dusting the BGO with a fine white abrasive powder (manufactured under the name Microgrit by Micro Abrasives Corporation of Westfield, MA) did not increase the signal strength. This should have been a good technique as powders of alumina or magnesium exoide are often used as reflectors in sodium iodide assemblies. However, those assemblies use a thick (approximately 1/16 inch) packing of powder which could not be duplicated in the laboratory.

TABLE II

Comparison of Various Reflective Coatings on Scintillation Pulse Height of a 25mm Crystal of BGO and a 38mm x 25mm NaI(Tl) Scintillator for .511 MeV Gamma Radiation

Condition of Scintillator	Pulse Height (volts) BGO	NaI(Tl)
no coupling oil	.26	4.6
coupling oil	.52	7.6
oil and aluminum foil (dull side in)	.66	
(shiny side in)	.70	
oil and dusted with Microgrit powder	.50	
oil, Microgrit powder and aluminum foil	.60	
oil and white (typing) correction fluid	.56	
oil and black electrical tape	.26	

$$\frac{\text{BGO signal strength}}{\text{NaI(Tl) signal strength}} = \frac{.70 \text{ volt}}{7.6 \text{ volt}} = 9.2\%$$

Not unexpectedly, a wrapping of black vinyl (electrical) tape acted as a black body absorber, increasing the photon loss through the wrapped surfaces. The BGO crystal prepared in this manner had a much lower signal output than did a bare crystal. A similar response was observed after spraying the crystal's sides and top surface with a metallic lacquer paint. It had been hoped that the metallic paint would act as a specular reflector, but such was not the case. A thin layer of this paint was applied to the BGO at its interface with the photomultiplier tube in an effort to get more photons out of the scintillator crystal and into the photocathode; but apparently even the thin layer was too thick, absorbing the photons and eliminating the output signal.

Resolution measurements of the .511 MeV annihilation gamma from sodium-22 using a fragment of BGO, provided a similar analysis of the effectiveness of different crystal preparations. These results are summarized in Table III. Again, a definite increase in resolving power was achieved by wrapping the crystal with aluminum foil. The experiment with a titanium coating involved the vacuum deposition of titanium onto the sides and irregular top surface of the BGO fragment. A marked decrease in resolution accompanied this deposition. Other researchers have noted adverse effects from metallic plating, but the theoretical aspects of this phenomenon are not understood. It was noted that the smooth cleavage surfaces of the BGO fragment received a specular coating of titanium whereas the frosted side walls had a duller coating. In an effort to

TABLE III

Effect of Reflective Coating on Resolution of .511 MeV Gamma Radiation by a BGO Fragment

Reflective Coating	Resolution* (%)
(oil coupling only)	29.9 ± .8
Aluminum foil	21.1 ± .9
Metallic paint	> 50
Microgrit powder and aluminum foil	20.9 ± .1
Titanium on top and sides	35.1 ± 3.9
on top	29.8 ± 1.8
on top with aluminum foil	26.9 ± 1.3
All surfaces etched in HCl	23.7 ± 1.5
Etched surfaces and aluminum foil	17.0 ± .7

*All determinations of resolution were based on a limited sample of 2 or 3 measurements, except for the last entry which was confirmed by six measurements.

retain only the specular nature of the titanium deposit, the coating was abrasively removed from the side walls. This alteration produced an improved resolution, which was further enhanced by the addition of an aluminum foil wrapping. All hopes for the potential of this titanium reflector were destroyed when another significant improvement was achieved with the complete removal of the titanium. Unfortunately, the metal adhered tenaciously to the BGO and had to be removed by immersion in hydrochloric acid. This process etched the entire crystal including the end window. However, the results were very rewarding. By wrapping the etched crystal in aluminum foil, a resolution of 17.0 ± .7% (at .511 MeV) was attained; the best performance to date for this fragment.

While performing resolution measurements on fragments from the original BGO crystal, it was amazing that the small pieces could perform as well as they did. It was even more astounding to realize that these measurements often exceeded those from the original crystal.

With inorganic halide scintillators, e.g., NaI(Tl), an optimum size crystal would be one which completely captures the incident radiation while minimizing the volume through which the scintillations must propagate in order to reach the photomultiplier. Any excess propagation distance subjects the scintillation photons to absorption losses. This self-absorption is thought to be negligible in a BGO crystal because of the large Stokes shift between the excitation and

fluorescent spectra. However, the self-absorption would explain the better resolution from small crystals when analyzing radiations of relatively low energy (less than 1 MeV).

Another consideration in explaining this effect is the influence of crystal geometry. The unique construction of the top surface on the fragment may be more effective in reflecting scintillations toward the end window at angles less than the critical angle than is the geometry of a regular cylinder. Because the fragment's top surface is basically a cleavage along a crystallographic plane, Bragg scattering may also exert an influence in this situation.

This phenomenon is still unresolved, and is an area worthy of additional investigation.

The resolution measurements obtained during this study are presented in Table IV and are compared to resolution values which were reported previously in the literature. Other sources appear to have obtained slightly better resolution with their BGO crystals (and their reflector geometries), but fragments of BGO with aluminum foil wrapping appear to be within experimental error of the best reported results.

C. RADIATION DAMAGE

Samples of bismuth germanate and thallium activated sodium iodide were exposed to 100 MeV electrons from the Naval Postgraduate School LINAC to determine the relative resistance of these crystals to radiation damage. Both

TABLE IV

Observed Values of Resolution from
Bismuth Germanate Crystals

Radiation Source	Whole Crystal	Crystal Fragments	Literature Values
Cesium-137	19.04 ± .28%	15.7 ± .18%	15% [Ref. 12]
			15% [Ref. 6]
			15.4% [Ref. 13]
Sodium-22			
.511 MeV	21.89 ± .52%	16.63 ± .57%	16% [Ref. 12]
			16.5% [Ref. 6]
1.27 MeV	13.76 ± .65%	11.30 ± .62%	10.5% [Ref. 6]
Cobalt-60			30% [Ref. 12]
			11.8% [Ref. 13]

scintillators produced copious amounts of visible light during the irradiation period. The photograph of Figure 14 was made to demonstrate this point and required that the electron beam current be reduced by several orders of magnitude to prevent the intense light from saturating the video system and photographic film.

For economic reasons a functional fragment from the broken BGO crystal was deemed sufficient for the radiation damage assessment. During irradiation this fragment was positioned so that that electron beam struck part of the original cylindrical surface slightly above the end window, thereby incurring the maximum possible propagation distance for shower containment with this particular fragment. The geometry of this fragment is illustrated in the photograph of Figure 12.

Since sodium iodide scintillators are employed most frequently in a manufactured configuration with glass windows and metallic casings, an assembly of this type (Harshaw 6D4) was chosen as a standard against which the radiation damage of BGO could be evaluated. While it was desired to evaluate the radiation resistance of the sodium iodide assembly as a whole, care had to be exercised not to prejudice the results by taking undue advantage of some of the assembly's weaker components. A definite system vulnerability had been revealed in a previous experiment when a similar assembly was irradiated for five minutes and the

crystal cracked, apparently from thermal stress. This crack produced such an extent of reflection at the grain boundary that the final signal bore no resemblance to the signal from a mechanically sound crystal. The assembly was useless for further analysis. Another liability of sodium iodide assemblies was revealed when such an assembly was irradiated through the end window, and glass in the region of beam impact was rendered opaque in the process. This darkening of the glass impedes scintillation transport into the photomultiplier tube and will reduce resolution based on statistical considerations alone, without providing any information about changes in the scintillator material proper. Accordingly, for this research in radiation damage analysis the sodium iodide assembly was oriented so as to have the electron beam strike the cylindrical surface at a height approximately two thirds of the distance away from the glass window. It was hoped that this geometry would contain the shower while minimizing any glass exposure with its subsequent discoloration. After several irradiation sequences a slight darkening of the glass was noted where the shower had expanded opposite the impact point to encompass the glass. For subsequent exposures the assembly was rotated from its original alignment in order to average any effects of glass discoloration.

The only optical effect observed in the bismuth germanate crystal was a slight peach hue which appeared after the two most intense exposures and faded away within a day or two.

This coloration appeared to be uniformly dispersed throughout the crystal and no adverse effects were noted.

Prior to exposure these scintillators were evaluated for resolution of the .66 MeV gamma radiation from cesium-137. After each irradiation the resolution was measured at periodic intervals to determine the change caused by the latest exposure and to observe any recovery with time. Table V summarizes the exposure history and resolution as a function of time for the BGO fragment. Similar data for the NaI(Tl) scintillator are presented in Table VI. Figures 15 and 16 graphically depict this same information on a continuous time scale from the beginning of the irradiation sequence.

To properly assess the amount of radiation damage inflicted by these experiments, it is important to understand the damage mechanism. The electrons per se do not have much of an effect on the crystal. However, as the high energy electrons are decelerated in the target material, they emit wide band bremsstrahlung radiation which can cause photon activation of the target nuclei. The predominant process noted was a gamma-neutron (γ,n) reaction wherein the gamma (bremsstrahlung) radiation raises a nucleus to an excited state which then decays by neutron emission. For target nuclei of high atomic number the gamma-proton and gamma-multiple particle reactions also have significant cross sections and were actually observed in the photon activation of BGO. The products of these activations are, in general, radioactive. Whenever an irradiated

TABLE V

Exposure History and Resolution of Bismuth Germanate

Time (hours)	Electron Beam Current (amps)	Beam Duration (sec)	Latest Exposure (No. of 100 MeV electrons)	Cumulative Exposure	Resolution (%)
0					15.67±.18
0	1.5×10^{-7}	60	5.8×10^{13}	5.8×10^{13}	
25.5					18.77±.41
31.5					18.37±.32
46					17.60±.34
70					16.26±.14
72.5	1.5×10^{-7}	67	6.4×10^{13}	1.2×10^{14}	
78.5					19.09±1.09
94.5					21.16±.43
122.5					20.17±.21
167.5					19.75±.27
192.5	7.7×10^{-8}	250	1.2×10^{14}	2.4×10^{14}	
198.5					21.13±1.56
214.5					21.07±.32
239.5					18.95±.19
262					18.32±.16
289.5					20.14±.45
384.5	9.2×10^{-8}	1200	6.9×10^{14}	9.3×10^{14}	
432.5					15.41±.85
483.5					20.22±.64
553.5					20.82±1.03
599.5					18.66±.32

TABLE VI

Exposure History and Resolution of Sodium Iodide

Time (hours)	Electron Beam Current (amps)	Beam Duration (sec)	Latest Exposure (No. of 100 MeV electrons)	Cumulative Exposure	Resolution (%)
0					10.1 ±.1
0	4.6×10^{-8}	30	8.6×10^{12}	8.6×10^{12}	
2					11.7 ±.7
21					11.5 ±.4
92					10.33±.16
93.5	4.6×10^{-8}	30	8.6×10^{12}	1.7×10^{13}	
94.5					10.35±.46
115.5					10.83±.35
142					10.62±.19
162					11.18±.04
164.5	1.5×10^{-7}	60	5.8×10^{13}	7.5×10^{13}	
186					11.36±.71
195					12.23±.79
210.5					11.09±.80
234					11.59±.65
237	1.5×10^{-7}	60	5.8×10^{13}	1.3×10^{14}	
244					16.20±1.18
260					15.12±1.04
285					14.69±.91
329					13.96±1.01
357	7.7×10^{-8}	250	1.2×10^{14}	2.5×10^{14}	
384					19.69±2.73
403					15.76±.94
427.5					20.89±2.85
455.5					15.66±.81
909					14.50±1.55

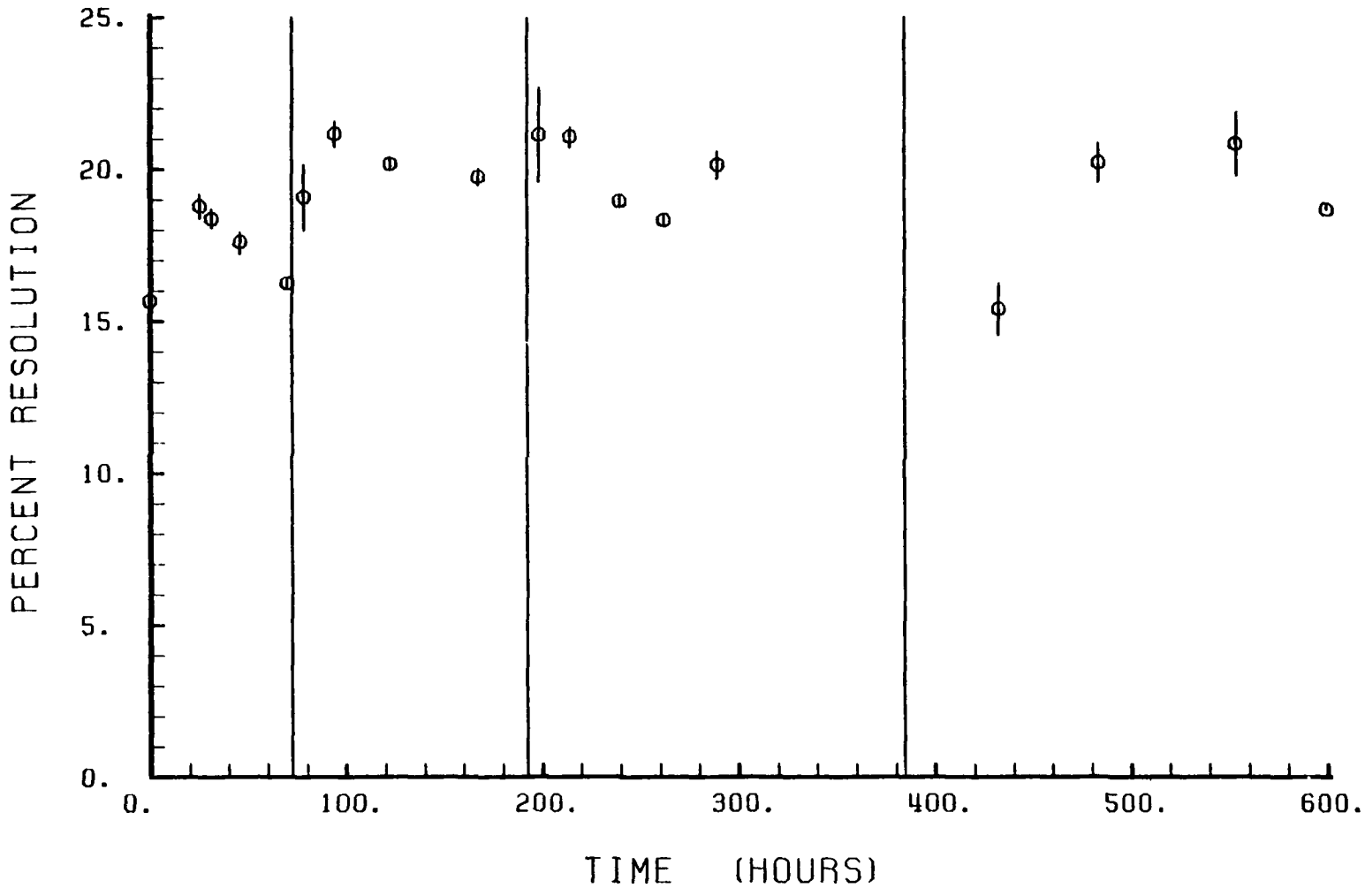

Figure 15. Resolution of Cesium-137 by Radiation Damaged Bismuth Germanate

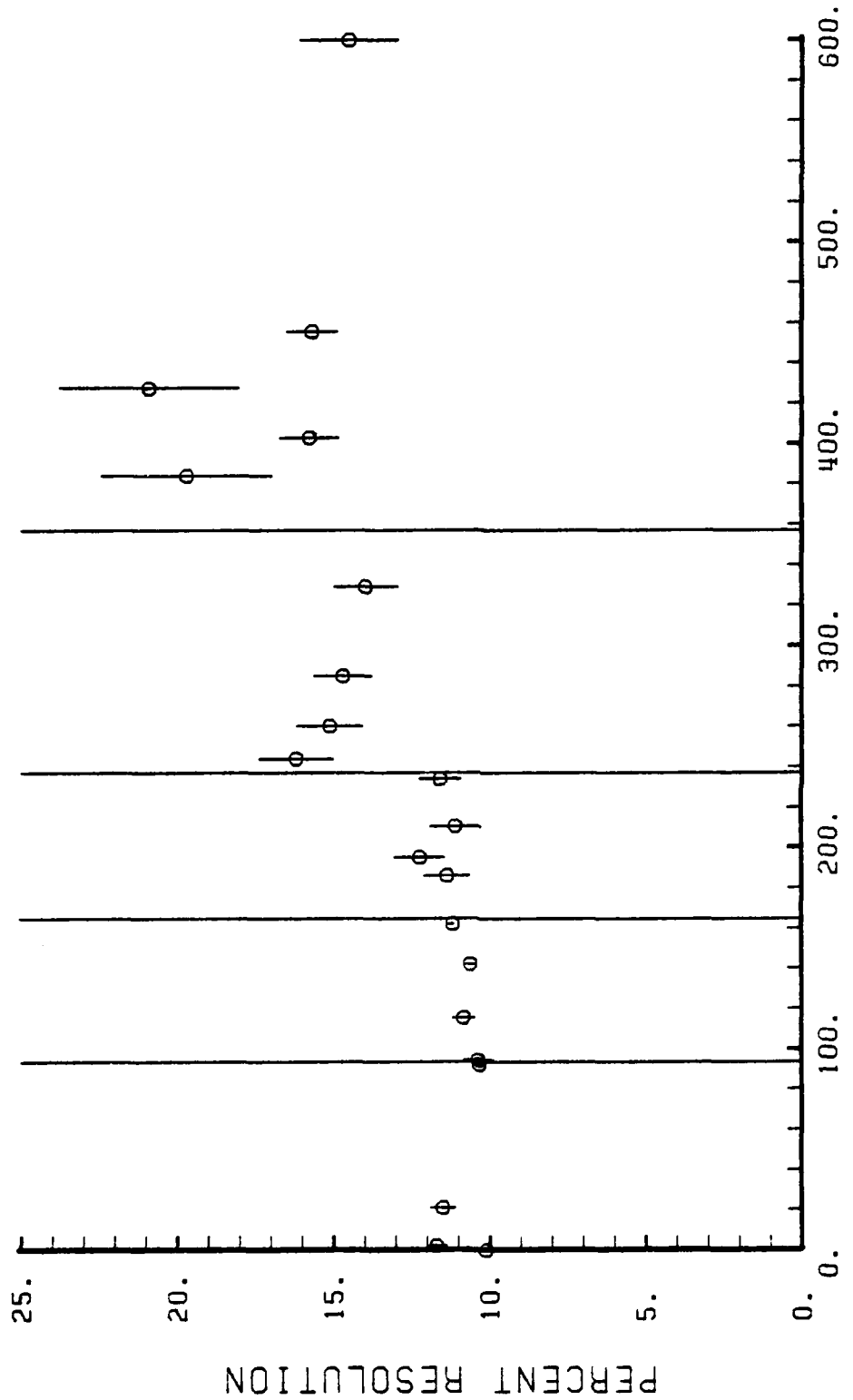

Figure 16. Resolution of Cesium-137 by Radiation Damaged Sodium Iodide

scintillation crystal is subsequently used for detection or analysis of external radiation, it will also respond to its own internal radioactivity.

Treating the "hot" scintillator crystal as a radioactive source material, its decay radiations were analyzed by a (non-irradiated) 3" x 3" sodium iodide detector. Table VII summarizes the results of this pulse height analysis for bismuth germanate [Ref. 11] and sodium iodide. Representative spectra from these analyses are shown in Figures 17 and 18.

The bismuth germanate's activity was predominantly due to activation of the germanium. Initially, there was a rather high activity which was determined to have a two minute half life and consequently attributed to oxygen-15, but because of its short half life it had decayed to inconsequential amounts prior to the resolution measurements of this experiment. After several days the minor amount of bismuth-206 which was formed became significant, due to the relative decay of all other isotopes. The decay of radioactivity in BGO is a time dependent function with an initial rate of 2 minutes (oxygen), intermediate rates on the order of 14 hours for the germanium products, and finally at 6 days due to the bismuth. The activity in sodium iodide was identified as being due to the formation of iodine-127 and its subsequent decay with a thirteen day half life. It was interesting to note the absence of characteristic gamma decay radiations from

TABLE VII

Radioactive Species in Photon Activated Scintillator Crystals of Bismuth Germanate and of Sodium Iodide

Scintillator Crystal	Observed Gamma Energy (MeV)	Emitting Nuclide	Half Life	Probable Formation Mechanism
BGO	.293	Ga^{73}	4.8 hr	Ge^{74} (γ,p) Ga^{73}
	.511	(unknown positron emitters)		
	.644 .901 2.191 2.489	Ga^{72}	14.1 hr	Ge^{73} (γ,p) Ga^{72} Ge^{74} (γ,np) Ga^{72}
	1.104	Ge^{69}	39.2 hr	Ge^{70} (γ,n) Ge^{69}
	1.720	Bi^{206}	6.24 day	Bi^{209} $(\gamma,3n)$ Bi^{206}
NaI(Tl)	.380 .663 .88 1.42	I^{127}	13 day	I^{128} (γ,n) I^{127}

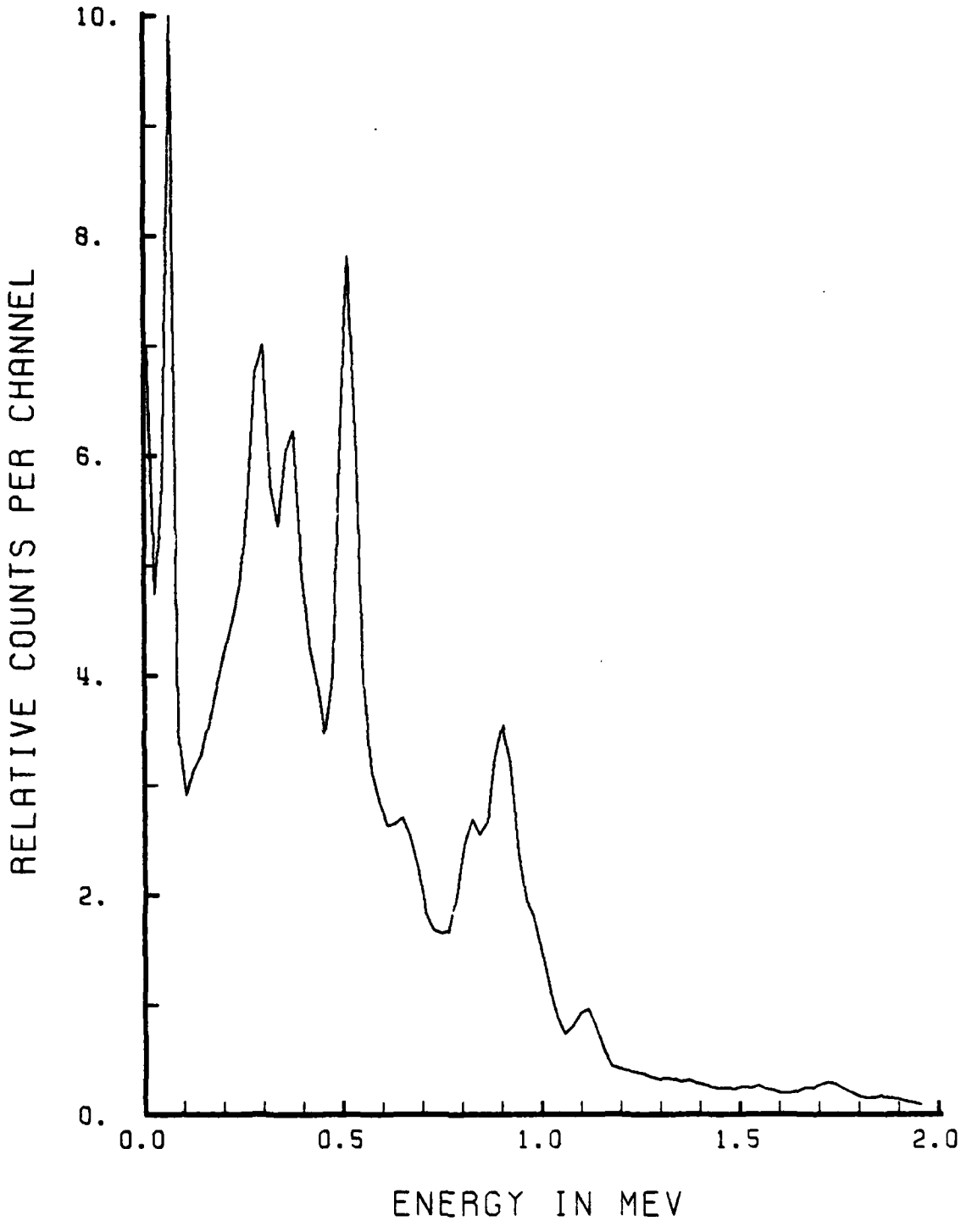

Figure 17. Pulse Height Spectra for a Source of Activated Bismuth Germanate Using a Non-radiated 3"x3" Sodium Iodide Scintillator Crystal

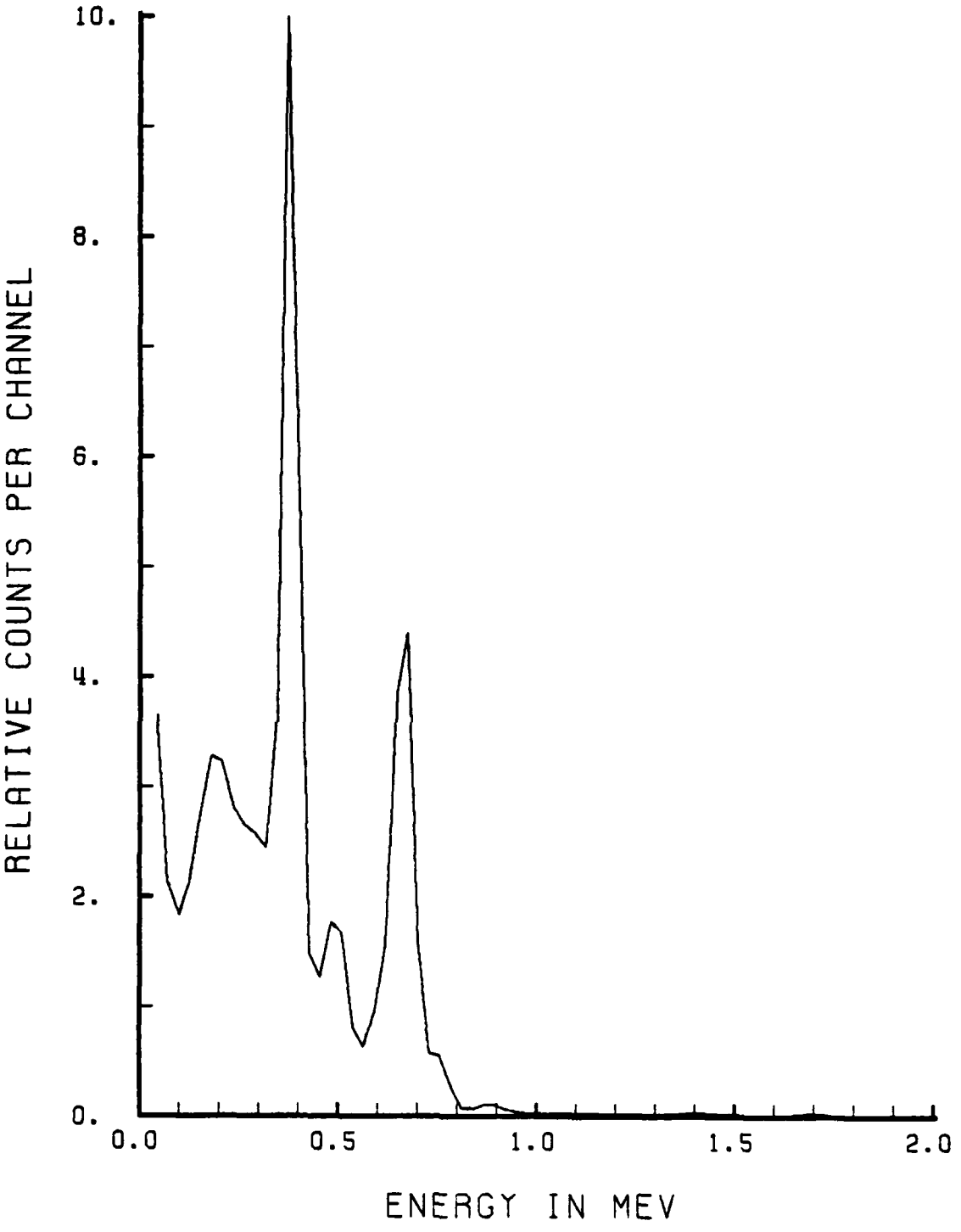

Figure 18. Pulse Height Spectra for a Source of Activated Sodium Iodide Using a Non-radiated 3"x3" Sodium Iodide Scintillator Crystal

aluminum which would have indicated that the casing or reflector packing had become activated. This considerably slower decay in the internal radiation of sodium iodide became a significant factor when assessing the post-irradiation recovery in resolution relative to BGO.

When accumulating a pulse height spectrum of low level source material, it is important to correct for background radiation. The cesium-137 source used in this study had a high activity of approximately two microcurries, and produced such large count rates when placed directly on the scintillator crystal that the background could safely be ignored within the region of interest (.66 MeV). However, after irradiation both types of scintillator crystals had background levels, from absorption of internal radioactivity, that were quite substantial relative to the cesium source and background subtraction again became essential. Figure 19 demonstrates the relative size of this background (24 hours after a total exposure of 1.3×10^{14} electrons) to the gross signal of cesium plus background. The vertical scale for these two figures are drawn to the same scale. For the BGO fragment the gross curve is more than double the counts for the background curve, whereas the sodium iodide gross curve is practically buried in a much larger background. In the sodium iodide case, subtracting two very large numbers to obtain the net cesium count, yields a number with fewer significant digits and a greater uncertainty than can be obtained for the widely separated curves of the bismuth germanate spectra. A

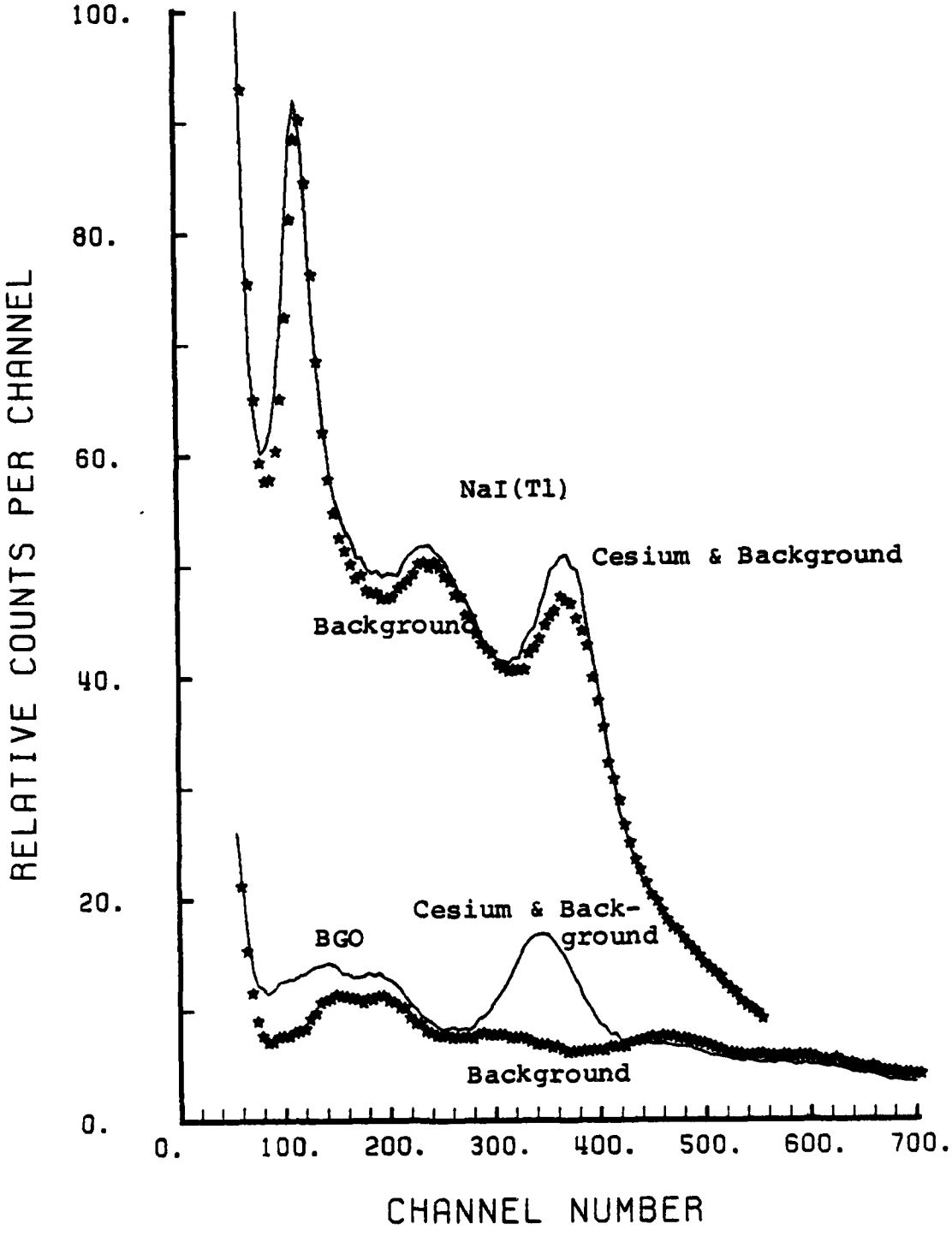

Figure 19. Background and Cesium-137 Spectra from Bismuth Germanate and Sodium Iodide 24 Hours after an Exposure to 1.2×10^{14} Electrons of 100 MeV

comparison of the two net cesium spectra (Figure 20) clearly shows the BGO response has a shape closer to the pre-irradiation spectrum and that there is less data scattering along the BGO curve. (The difference in channel numbers for the cesium photopeak in these two cases is a function of the amplifier gain. A reproducable gain setting was selected for each type of scintillator so as to keep the spectra on the same scale, but no attempt was made to have the peaks coincide. The BGO gain setting was approximately eight times greater than for the NaI(Tl).)

The buildup of internal radiation as measured twenty-four hours after exposures of 1.2×10^{14} and 2.4×10^{14} electrons is contrasted in Figure 21 for the two types of scintillators. Again, the correlation of channel numbers between the BGO and NaI(Tl) spectra is only approximate, but the quantity of detected events reflects the greater activity level in NaI(Tl).

The relative decay of induced radioactivity is graphically depicted in Figure 22 for the times of six, twenty-four and ninety-six hours after exposures of 2.4×10^{14} electrons of 100 MeV energy. Here one can readily appreciate the lesser activity and faster decay of bismuth germanate.

When measuring the resolution of radiation damaged scintillators, the "percent dead time" of the pulse height analyzer assumed a significant role. Dead time refers to the time interval after a signal pulse when the PHA is performing

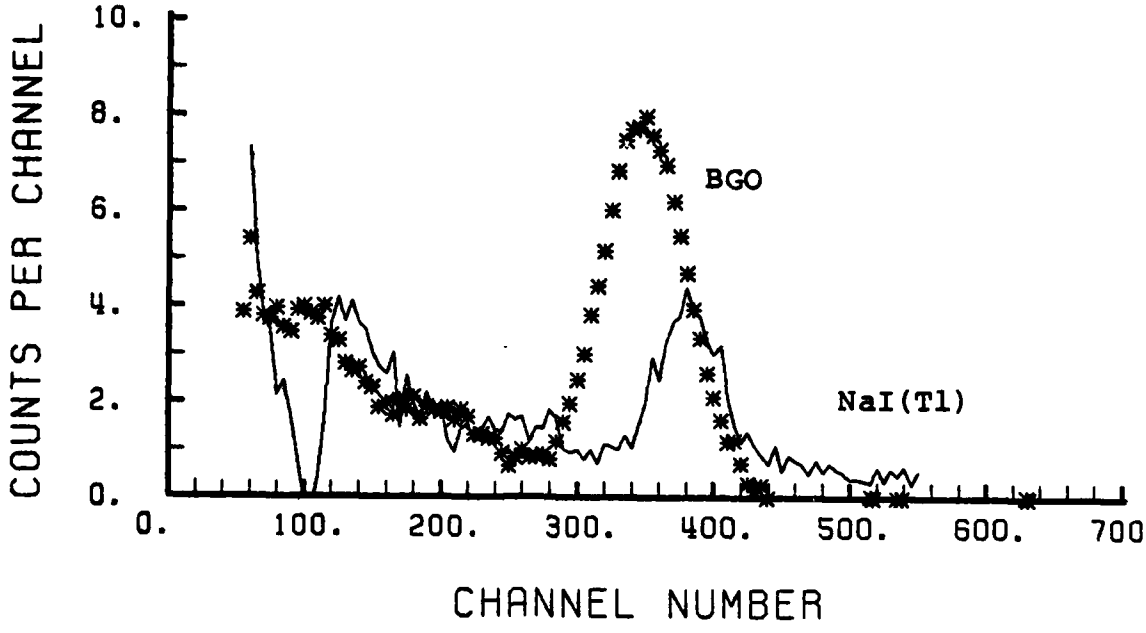

Figure 20. Comparison of the Net Cesium Spectra from Crystals of Bismuth Germanate and Sodium Iodide 24 Hours After an Exposure to 1.2×10^{14} Electrons of 100 MeV

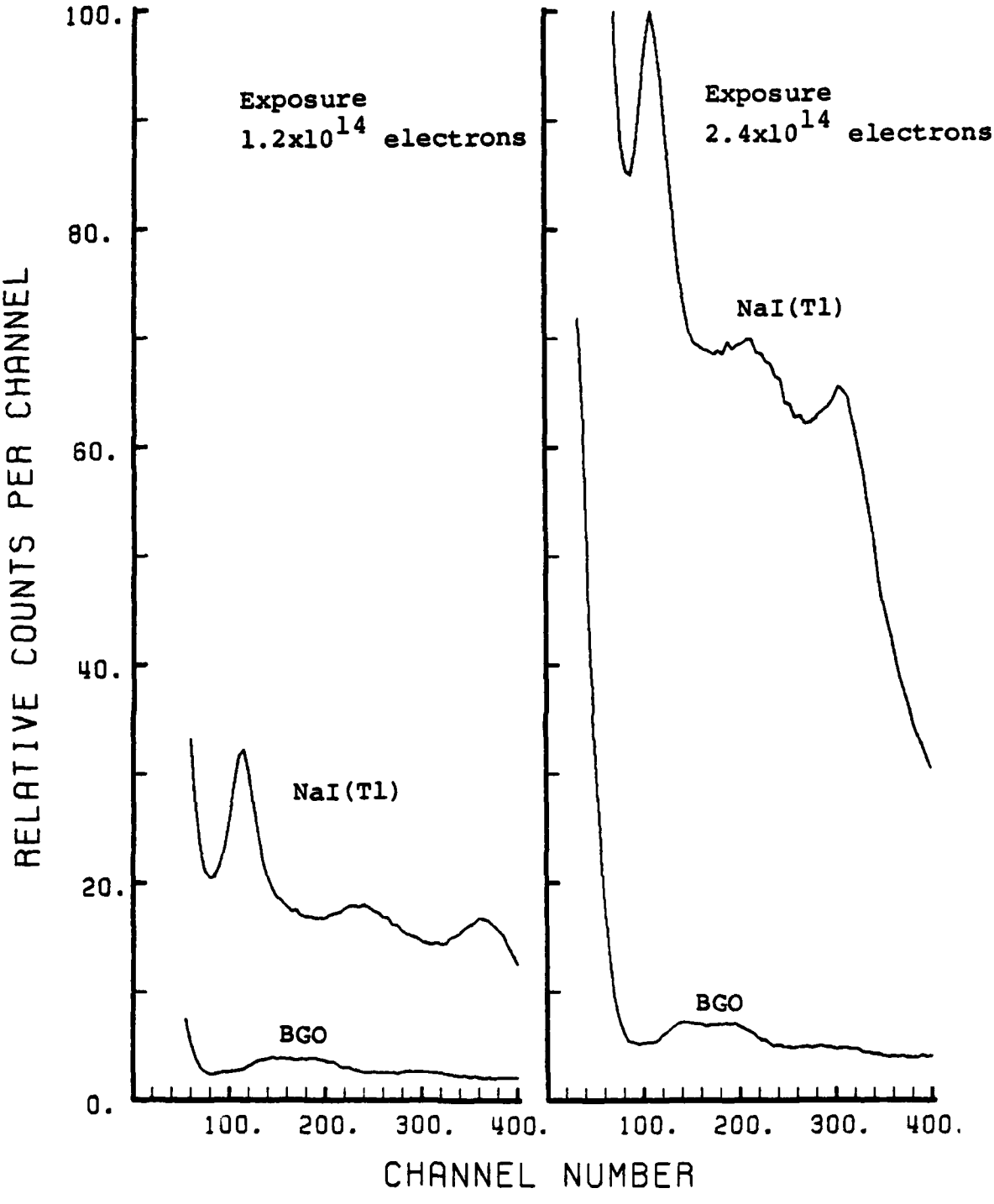

Figure 21. Induced Radioactivity in BGO and NaI(Tl) at 24 Hours after Total Exposure to 1.2×10^{14} and to 2.4×10^{14} Electrons of 100 MeV

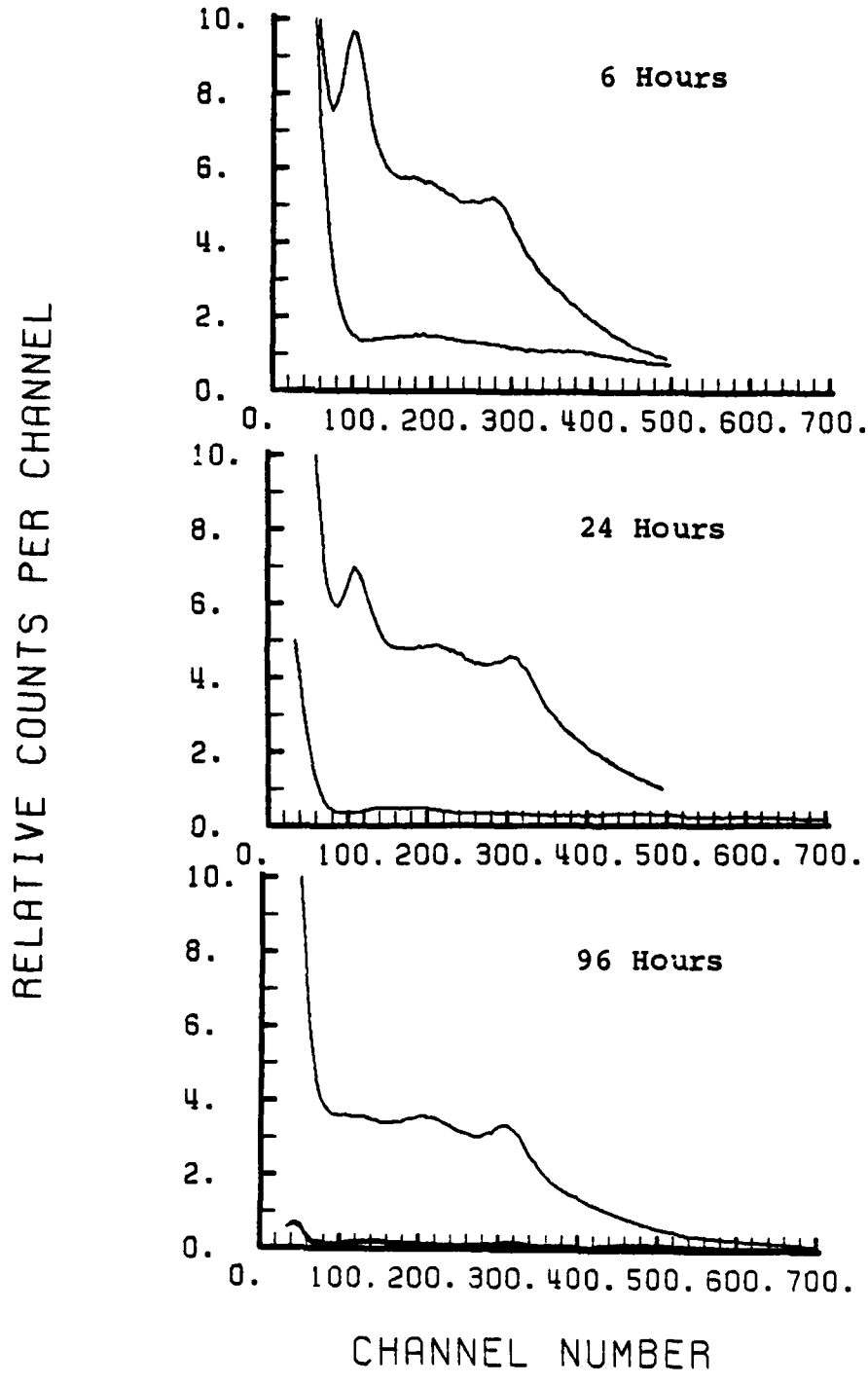

Figure 22. Decay of Induced Radioactivity in BGO and NaI(Tl) Scintillators at Times of 6, 24 and 96 Hours after Exposure to 2.4×10^{14} Electrons of 100 MeV

the analog to digital conversion of that pulse and storing it in memory. Additional acquisition of signal pulses is not possible during this processing time. Percent dead time is the ratio of the accumulated dead time to the total time during which the counting sample was being acquired. Normally, the time between radiation detection events is long compared to the processing time and the percent dead time is quite low. However, when analyzing a radioactive material with a radioactive scintillator, both sources contribute to the counting rate and the time between detection events becomes smaller and the percent dead time increases. The lower limit discriminator (LLD) control on the PHA is used to establish a minimum value of signal strength for event detection. Raising the LLD will prevent the PHA from registering those events of low signal strength (low energy) and will reduce the percentage of dead time.

It was observed that at high rates of dead time the number of detected events (for those energies above the low limit cut-off) was affected by the setting of the LLD control. Even the channel number into which these events were assigned was subject to shifting as the dead time increased. To avoid, or at least minimize these errors the LLD had to be progressively increased as the scintillator became more and more radioactive in the irradiation sequence. This meant that less and less of the low energy end of the pulse height spectrum was being recorded, until eventually even the photopeak

would be eliminated. Obviously, some error had to be accepted or there would have been no signal left to analyze. The scattering of data in Figures 15 and 16 for high exposures reflects this consequence of high counting rates.

A related problem was faced in trying to acquire resolution data on the activated sodium iodide. As was demonstrated in Figure 19, there was only a small difference between the spectra for background and for the background plus cesium source. Also, the photopeak for the cesium-137 occurred very close to a maximum in the background spectrum. If there was any change in the correlation of energy to channel number during the time lapse between the acquisition of these two spectra, the small net contribution from the cesium source could very easily be negated by the large difference in background level corresponding to a slight shift in energy assignment. Slight shifts in operating conditions were unavoidable because the high voltage to the photomultiplier had to be turned off every time the light-tight box containing the scintillation apparatus was to be opened to make a change in the position of the cesium source material. After reconnecting the high voltage and allowing time for equilibrium to be established, there was enough change in operating conditions so that the spectrum obtained by subtracting background from the gross cesium count was often meaningless. There were many days when no resolution measurements of irradiated sodium iodide could be made, despite the most persistent efforts.

It is anticipated that a similar problem would be encountered with bismuth germanate if the radiation exposures continued until its background activity was in the same proportion to the cesium signal.

VIII. CONCLUSIONS

Optimum resolution was achieved from a bismuth germanate scintillator when using a reflector consisting of a wrapping of aluminun foil. This showed a small but significant increase in resolution, 13% as contrasted to 16% for a reflector made from alumina powder.

In the region of .5 MeV to 1.3 MeV, the energy resolution of BGO results in photopeaks which are considerably wider than for thallium activated sodium iodide detectors, namely resolutions of 15.7% for BGO versus 10.1% for NaI(Tl) at a gamma energy of .66 MeV.

Bismuth germanate is more resistant to damage from 100 MeV electrons than is sodium iodide, and any activity induced in bismuth germanate will decay faster than corresponding activity in sodium iodide (half lives on the order of tens of hours for BGO and thirteen days for sodium iodide).

Bismuth germanate does not require a glass window and protective case as does the hydroscopic sodium iodide. Consequently bismuth germanate is free from the problems associated with glass discoloration in a radiation environment.

Although not immune to mechanical damage, bismuth germanate is superior to sodium iodide in this category. Additionally, there was no evidence of thermal stress in irradiated bismuth germanate, whereas one crystal of sodium iodide was destroyed by this mechanism.

As a final note, better resolution was observed from a fragment of a broken BGO crystal as compared to the whole crystal. This suggests that the relatively poor resolution from BGO might be associated with crystal size or geometry, but further experiments to confirm this hypothesis have not been performed.

LIST OF REFERENCES

1. Kaplan, I., Nuclear Physics, Addison-Wesley, 1962.

2. Curran, S. C., Luminescence and the Scintillation Counter, Academic Press, 1953.

3. Enge, H. A., Introduction to Nuclear Physics, Addison-Wesley, 1966.

4. Fenyves, E. and Haiman, O., The Physical Principles of Nuclear Radiation Measurements, Academic Press, 1969.

5. Knoll, G. F., Radiation Detection and Measurement, Wiley, 1979.

6. Buskirk, F., and others, "Energy Resolution Measurements on a Large Single BGO Crystal from 1 MeV to 50 MeV", IEEE Transactions on Nuclear Science, V. NS-29, pp. 346-350, February 1982.

7. Weber, M. J. and Monchamp, R. R., "Luminescence of $Bi_4Ge_3O_{12}$: Spectral and Decay Properties", Journal of Applied Physics, V. 44, pp. 5495-5499, December 1973.

8. Bortfeld, D. P. and Meier, H., "Refractive Indices and Electro-Optic Coefficients of the Eulitities $Bi_4Ge_3O_{12}$ and $Bi_4Si_3O_{12}$", Journal of Applied Physics, V. 43, pp. 5110-5111, December 1972.

9. Engstrom, R. W., Photomultiplier Handbook, RCA Corp., 1980.

10. ORTEC Inc., Experiments in Nuclear Science, 2d ed., 1976.

11. Fisher, W. A., Instrumental Photon Activation Analysis Using the Electron Linear Accelerator at the Naval Postgraduate School, M.S. Thesis, Naval Postgraduate School, Monterey, California, 1982.

12. Nestor, O. H. and Huang, C. Y., "Bismuth Germanate: A High-Z Gamma-ray and Charged Particle Detector", IEEE Transactions on Nuclear Science, V. NS-22, pp. 68-71, February 1975.

13. Evans, A. E., "Gamma-ray Response of a 38mm Bismuth Germanate Scintillator", IEEE Transactions on Nuclear Science, V. NS-27, pp. 172-175, February 1980.

BIBLIOGRAPHY

Diachok, O. I. and Mayer, W. G., "Electromechanical Properties of Bismuth Germanate $Bi_4(GeO_4)_3$", Transactions on Sonics and Ultrasonics, pp. 219-221, October 1969.

Drake, D. M., Nilsson, L. R., and Faucett, J., "Bismuth Germanate Scintillators as Detectors for High Energy Gamma Radiations", Nuclear Instruments and Methods, pp. 313-317, 1981.

Kirkbride, I., Coyne, D., and Cavalli, M., BGO Report, lecture notes from briefing to Crystal Ball Group, Stanford University.

Nitsche, R., "Crystal Growth and Electro-Optic Effect of Bismuth Germanate, $Bi_4(GeO_4)_3$", Journal of Applied Physics, V. 36, pp. 2358-2360, August 1965.

Patterson, H. W. and Thomas, R. H., Accelerator Health Physics, Academic Press, 1973.

Richtmyer, F. K., Kennard, E. H., and Cooper, J. N., Introduction to Modern Physics, 6th ed., McGraw-Hill, 1969.

Spinks, J. W. T. and Woods, R. J., An Introduction to Radiation Chemistry, 2d ed., Wiley, 1976.

Weinstein, R., Interaction of Radiation with Matter, McGraw-Hill, 1964.

INITIAL DISTRIBUTION LIST

		No. Copies
1.	Defense Technical Information Center Cameron Station Alexandria, Virginia 22314	2
2.	Library, Code 0142 Naval Postgraduate School Monterey, California 93940	2
3.	Department Chairman, Code 61Dy Department of Physics Naval Postgraduate School Monterey, Californa 93940	1
4.	Professor Fred Buskirk, Code 61Bs Department of Physics Naval Postgraduate School Monterey, California 93940	3
5.	Headquarters, Department of the Army Military Personnel Center Attn: DAPC-OPS-CM 200 Stovall Street Alexandria, Virginia 22332	1
6.	Deputy Under Secretary of the Army for Operations Research Room 2E261, Pentagon Washington, D.C. 20310	1
7.	Lt. Wayne Fisher, USCG Coast Guard Headquarters - EOE Acoustics and Optics Branch Washington, D.C. 20593	1
8.	Cpt. Robert Cooke 1042 Innsbruck Livermore, California 94550	3

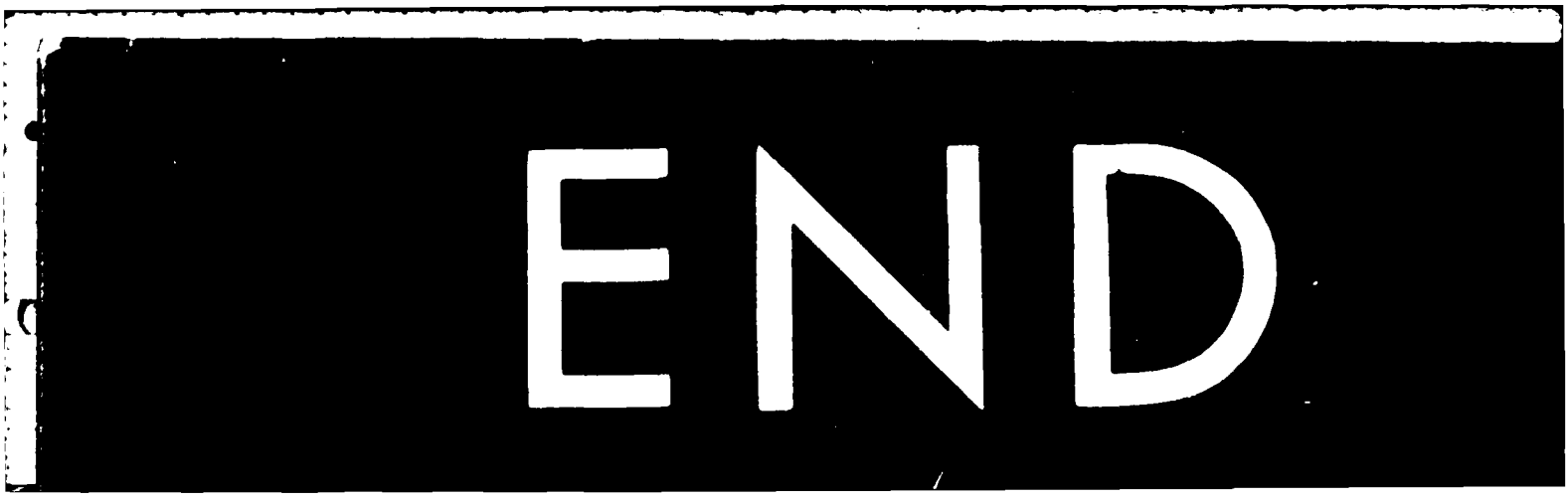
END